

Probabilistic Risk Assessment (PRA) for Sustainable Water Resources Management: A Future Flood Inundation Example

Nick Martin^{1,*}, Francisco Peña^{2,3} and David Powers⁴

¹ Vodanube LLC, Fort Collins, CO, USA

² Galt Group Inc., West Palm Beach, FL, USA

³ UNESCO Chair on Sustainable Water Security, Miami, FL, USA

⁴ Security & Resilience Program, Bureau of Overseas Buildings Operations, U.S. Department of State, Washington, DC, USA

Correspondence*:

Corresponding Author

nick.martin@alumni.stanford.edu

2 ABSTRACT

Traditional engineering practice provides a backward looking approach that develops design bases from historical observations and past experience. Rapidly changing climatic conditions mean that historical observations are insufficient for future planning, which must consider inherent lack of knowledge related to future conditions. This focus on the past, despite observed, ongoing, and rapid change, has created unsustainable resources management approaches where most of the extra costs generated by limitations of current and historical engineering design and regulatory requirements will be born by future generations. A probabilistic risk assessment (PRA) for future flood inundation is presented to examine sustainability-related solutions for the scenario where a regulatory compliant land use configuration is unsustainable when planning uncertainty considerations, related to future climate and weather, are applied. Weather attribution provides scientific and future uncertainty quantification for probabilistic climate description. This PRA provides support for sustainable decision making because the likelihood of inundation damage can be used to split total mitigation cost between current and future generations. PRA, as a tool, provides risk and sustainability assessment but is fundamentally limited for analysis and promotion of circularity because it does not include bonuses for benefits.

Keywords: uncertainty, probabilistic risk assessment (PRA), weather attribution, sustainability, circularity, flood inundation, climate change, water resources management,

1 INTRODUCTION

Sustainability can be defined as meeting the needs of the present without compromising the ability of future generations to meet their needs (Browne, 2022; United Nations, 2024; U.S. Chamber of Commerce Foundation, 2016). Inherent in the concept of sustainability is rationed exploitation and communal management of resources to ensure that today's activities do not significantly jeopardize quality of life in subsequent decades. Consequently, the concept of sustainability is a fundamental underpinning of engineering design considerations to protect against flood inundation and corresponding property damage

and of land use regulations developed to protect current and future beneficial uses and associated safety considerations.

Engineering practice focuses on meeting design bases to ensure that asset design and construction satisfies applicable regulatory requirements, standards, and guidelines. These design bases provide known targets as shown on Figure 1. Traditionally, engineering-related regulatory requirements, standards, and guidelines are developed from practitioner experience and historical observations in a fundamentally backward looking approach. Because there are known targets defined using past observations, engineering uncertainty focuses solely on accuracy and precision referenced to the target as displayed on Figure 1. This type of uncertainty can also be called exact value uncertainty because it assumed that the missing knowledge is high precision delineation of the bullseye.

Uncertainty is lack of knowledge. The scientific method uses hypothesis testing to refine the amount of knowledge and reduce uncertainty. For hypothesis testing, the underlying assumption is that the target values, or the “Truth” population in Figure 2, is only approximately known. Consequently, there is not a well defined target (as in Figure 1), and it is assumed that the true population is unknown and that the available estimates of the “Truth” population are biased, generating the “Biased Truth Estimate” sample in Figure 2. When a “Biased Truth Estimate” sample is used to constrain the “Truth” population, a range of values and likelihoods (or probabilities) should be used to describe certainty and uncertainty. The goal with a range of values to explicitly characterize uncertainty is to introduce sufficient estimate variability to account for the hypothesized amount of uncertainty as shown on Figure 2 Martin and White (2024).

Assuming that historical observations provide sufficient information, by themselves, to define the bullseye and thus looking to the past to plan for the future, works in a static environment where it is expected that what occurs next year will not exceed the range of occurrences during the last 30-, 50-, or 100-years. Unfortunately, it is evident that climate is evolving rapidly across the globe, new weather extremes are occurring every year, and the expected frequencies for extreme events are also increasing each year (IPCC, 2021; World Weather Attribution (WWA), 2024). Because weather and climate directly impact natural resources management and especially water resources management, a backward looking approach in a rapidly changing environment provides limited sustainable decision support.

For sustainable management of water resources, planning uncertainty needs to be used as the basis for engineering design and technology implementation. Planning uncertainty aggregates scientific and future uncertainties as shown on Figure 3. Scientific uncertainty, as depicted on Figure 2, describes and attempts to compensate for historical and present day knowledge limitations with augmented variability. Future conditions are unknown and include possibilities for conditions that are significantly different from present day and historical environments. The farther into the future, the greater the knowledge deficit for environmental conditions. The result is a “cone” of uncertainty for future conditions with the cone spreading, and uncertainty increasing, as progress into the future. In Figure 3, future uncertainty is the extra uncertainty, beyond what exists for present day, generated from the possibilities of occurrence of significantly different environments decades into the future.

There is a long history of engineering and scientific analyses that rely on the concept of planning uncertainty to address the likelihood of significant negative consequences related to natural resources management. Likelihood of negative consequences is risk, and the aerospace and nuclear industries have well developed probabilistic risk assessment (PRA) procedures and approaches that have been in widespread use since the 1980s and 1990s for safety and performance assessment. In aerospace, PRA is commonly used for manned space missions (Hsu and Railsback, 2004), and it is required for safety

assessment of reactor and waste storage construction and management in the nuclear industry. PRA is a comprehensive, structured, and logical analysis method aimed at identifying and assessing risks in complex systems for the purpose of cost-effectively improving safety and performance. In PRA, scenarios provide for characterization of fundamentally different future conditions, and thus PRA can explicitly incorporate future uncertainty (Stamatelatos et al., 2011).

PRA is mature technology and is still in widespread use in the aerospace (Stamatelatos et al., 2011; Pan et al., 2022) and nuclear and radioactive waste industries (Alkhatib et al., 2024; Lee et al., 2023; Kubo, 2023). For example, the U.S. Nuclear Regulatory Commission's Office of Nuclear Regulatory Research (NRC/RES) hosts an annual Probabilistic Flood Hazard Assessment (PFHA) Research Workshop. PFHA can include PRA but focuses broadly on probabilistic hazard assessment from flooding for nuclear energy related facilities. Additionally, PRA has been used recently to analyze risks from toxic materials in the environment (Han et al., 2023; Guadalupe et al., 2024; Ololade et al., 2023; Landquist et al., 2016; Sawe et al., 2021; Shen et al., 2024; Sheng et al., 2021; Stehle et al., 2013; Zhou et al., 2023), sequestration of hazardous materials via deep well injection (Martin et al., 2022; Rish, 2005), seismic hazards (Bernal et al., 2017; Salgado-Gálvez et al., 2017), and addition of fluoride to treated water supply (García-Montiel et al., 2023; Shahsavani et al., 2022).

In terms of considerations that are more "natural", rather than "industrial", resources, PRA has been applied to assess wildfire risk at the Wildland-Urban Interface (WUI) (Masoudvaziri et al., 2023) and from changing wildfire climate (Monge et al., 2023). It has also been employed to look at soil erosion from remote sensing data (Zhao et al., 2024) and soil slope stability related to dewatering (Wang et al., 2022). Martin (2021b,a) used PRA to analyze climate and land use and land cover (LULC) change impacts to water availability at the watershed scale.

This study provides an initial applied research phase implementation of PRA to support sustainable water resources management. Research goals are to analyze: 1) advantages PRA provides for consideration of sustainability concepts and 2) limitations generated from a focus on sustainability, generally, and implementation of PRA, specifically. To minimize preliminary phase study costs, a partially synthetic future flood inundation example scenario was developed to examine PRA for sustainability considerations.

The example scenario is a combination of real weather and climate data and analyses for the Frio River basin near Uvalde, Texas (TX) with a synthetic topography and land development configuration. Actual weather and climate data for this study site were analyzed as part of Martin (2023). This analysis identified that severe three-month drought has become five times more likely and that a 24-hour precipitation depth of 236 *mm* (which is approximately the historical 100-year, average recurrence interval event) has become four times more likely during the last 20 to 30 years. These large magnitude changes to expected drought and storm intensity create a situation where traditional backward looking engineering design considerations, and planning practice based solely on engineering considerations, produce land development that will be untenable, without continuous damage mitigation expenditure, for future generations.

A synthetic study site configuration was selected to generate the case where: 1) no flood inundation occurs under a historical design basis provided by a daily precipitation depth of 236 *mm* but that 2) flood inundation will occur starting with a daily precipitation depth of about 275 *mm*. The synthetic configuration, combined with actual weather and climate, provides a worked example of decision support for splitting mitigation costs between current and future generations and identifies the utility of PRA for sustainable resources management. Significant cost savings are realized using a synthetic site for this

exploratory study because topographic and as-built surveys are not required, and custom inundation damage curves for each asset in the study area do not need to be developed.

This example PRA for flood inundation demonstrates incorporation of planning uncertainty to sustainable water resources management considerations. Planning uncertainty description, related to future extreme weather generating flooding, is developed from weather attribution (Clarke and Otto, 2023; World Weather Attribution (WWA), 2024; van Oldenborgh et al., 2021; Philip et al., 2020). Property damage from inundation is the negative consequence, and the magnitude of property damage is cast to present day cost. Propagation of planning uncertainty through PRA provides probabilistic description of future damage magnitude, i.e., cost, based on recently observed weather extremes and updated likelihood for recurrence of these extremes during the next 30 to 45 years. Sustainability considerations are PRA-based decision support for what amount to spend now in order to limit the possibilities for future negative consequences and associated expenditures.

2 DATA AND METHODS

The principal method in this analysis is PRA, discussed in Section 2.1. It is a compound analysis of a series of events represented with an event tree. In this case, the event tree includes consideration of a probabilistic future climate description (see Section 2.2), computer model for simulating clear water inundation (see Section 2.3), stochastic channel obstruction events (see Section 2.4), and flooding damage cost estimation (see Section 2.5).

2.1 Probabilistic Risk Assessment (PRA)

The purpose of PRA is risk evaluation for risk management and decision making. Traditionally, it is applied to complex engineered systems and extends reliability engineering assessment. Reliability of an engineered, or designed, component is the probability that the component will not fail during a specified duration. The “mean time to failure” (MTTF) metric is a generally familiar reliability analysis outcome. In general, reliability analysis focuses on the design basis for a system and employs engineering uncertainty considerations (see Figure 1).

PRA extends reliability assessment to include planning uncertainty considerations (see Figures 2 and 3). The first comprehensive PRA was related to nuclear reactor safety and extended reliability engineering analysis to generate insight into how relatively frequent and minor accidents could initiate a complex chain of events leading to more severe consequences than some infrequent and major accidents (Stamatelatos et al., 2011). Subsequently, PRA has been employed as the basis for performance assessment of radioactive waste disposal and applied to analyze hazards across hundreds of thousands of years. This extremely long planning and analysis time frame requires explicit depiction of future uncertainty and planning uncertainty.

Risk related to decision making regarding complex, engineered systems encompasses scenarios, likelihoods, and consequences, and risk is the likelihood of negative consequences. Risk management is the reduction in frequency, or likelihood, of adverse scenarios, or accidents. Adverse scenarios are outcomes with negative consequences. Preventing accidents requires an understanding of the full chain of events that need to occur across multiple parts of a complex system to generate failure. Each sequence of events that can produce failure is a scenario. The risk for a particular scenario is the probability for system failure generating negative consequences. Use of risk assessment in decision making requires that uncertainty be addressed and quantified through assignment of likelihoods or probabilities to events

and that these likelihoods be conditionally propagated through the scenario to determine likelihoods for negative consequences (Stamatelatos et al., 2011).

System failure scenarios begin with an initiating event that represents change from desired system state. After initiation, the assessment proceeds by identifying pivotal events that may occur and that will exacerbate or mitigate scenario progression toward a full system failure and negative consequences. The sequence of pivotal events is represented with an event tree where each event represents a node in the progression of failure from the initiating event. At each node, an event occurs, or does not occur, that propels, or mitigates, the final consequences of the scenario. An individual event in an event tree can be represented with a fault tree, which provides detailed logical relationships between complex and basic component failures (Stamatelatos et al., 2011). In PRA, each event, in an event tree, and each fault, in a fault tree, is represented probabilistically to describe the likelihood of the event or fault occurring, and the uncertainty associated with occurrence, in isolation from the system.

2.1.1 Event Tree and Initiating Event

Figure 4 is the event tree for this PRA. System failure is flood inundation above the foundation elevation for one or more of the 44 houses in the synthetic site configuration shown on Figure 5. Foundation elevation for each house is provided on Table S1. Failure is evaluated by moving along the sequence of events from initiating event until determination of the amount of inundation (or of no inundation).

The initiating event is a daily precipitation depth greater than or equal to 236 mm (9.3 in), which is the 24-hour, 25-year recurrence rainfall estimate from Perica et al. (2018) for the Frio River basin. For context, the 24-hour, 100-year recurrence rainfall estimate from Hershfield (1963) for the Frio River basin is 233.7 mm (9.2 in). Hypothetically, the 233.7 mm precipitation depth would have been used as design criteria for the 1% probability annual exceedance flood event if the assets in the synthetic study site configuration (see Figure 5) were constructed between 1965 and 2000. Consequently, we assume that no flooding occurs from daily precipitation depths less than 236 mm. Comparison of the estimates provided by Perica et al. (2018) and Hershfield (1963) identifies that a rainfall intensity of 236 mm/day is four times more likely to occur under present day conditions than 30 to 40 years ago.

A collection of 1,000 future weather realizations is examined to obtain the collection of initiating events, and Section 2.2 details the generation of these future weather realizations. For each day within a realization, synthetic daily precipitation is compared to 236 mm to determine if an initiating event occurs. When the initiating event occurs, the initiating precipitation depth is scaled to a reach inflow discharge so that flood inundation can be simulated as discussed in Section 2.3.

A proportionality constant was derived to convert 236 mm of daily precipitation to a discharge of 180 m³/s-days. This proportionality constant (180 m³/s-days / 236 mm = 0.7627 m³/s-days / mm) is conceptually similar to the runoff coefficient, *C*, in the Rational Method (Chow et al., 1988), and it was selected because a 180 m³/s-days input discharge, with an obstruction height of 0.0 m, does not generate foundation inundation and system failure for the synthetic site configuration. In other words, no flood inundation results from 236 mm of daily precipitation depth (with no channel obstruction), which demonstrates that the bridge and houses were designed and built in compliance with the historical requirements of no flooding from the 24-hour, 100-year recurrence rainfall estimate of 233.7 mm from Hershfield (1963).

The second event in Figure 4 is obstruction height determination. Both branches from this event are evaluated with the inundation simulation model. The “Stochastic Obstruction Height” branch is selection

of an obstruction height from the probability distribution discussed in Section 2.4, and the “No Obstruction” branch is specification of no obstruction height, or an obstruction height of 0.0 *m*.

“Simulated Water Depth” provides the third and final event on Figure 4. Scaled inflow discharge is evaluated twice as part of this event because both “Bridge Obstruction” branches are simulated using the scaled inflow discharge from the initiating event. The modeling approach presented in Section 2.3 evaluates “Inundation” by comparing the simulated water surface elevation adjacent to each house to its foundation elevation to determine if there is inundation and flood damage.

When inundation and damage are simulated, there is system failure for one or more regulatory-compliant houses. Damage cost estimating is discussed in Section 2.5. Total damage cost is summed across all initiating events within each future weather realization. If there are four daily precipitation depth projections greater than or equal to 236 *mm* in realization number 47, then the total damage for realization number 47 is calculated as the sum of damage estimates from these four initiating events. The result is 2,000 (1,000 with no channel obstruction and 1,000 with a randomly sampled channel obstruction) total damage cost estimates from projected climate during 2024–2065 (42 years).

2.2 Future Weather and Climate Inputs

Martin (2023) provides 1,000 realizations of synthetic, daily weather for 2024–2065 for the Frio Basin that are constrained to reproduce: 1) five times more likely severe three-month drought, 2) four times more likely rainfall intensity of 236 *mm/day*, and 3) annual average precipitation depth observed from 1991–2020. The five times more likely severe three-month drought is based on a weather attribution study that is applicable to the Frio Basin (Schumacher et al., 2022). The four times more likely extreme rainfall intensity comes from comparison of Hershfield (1963) and Perica et al. (2018), as discussed in Section 2.1.1. The expectation for approximately constant annual average precipitation depth comes from analysis of localized constructed analogs (LOCA) downscaling of Coupled Model Intercomparison Project, Phase 5 (CMIP5) future climate projections (Martin, 2021b). These 1,000 realizations provide the projected future weather used to determine initiating event occurrence.

The synthetic weather series were created using a stochastic weather generator (WG) that was calibrated, or constrained, to produce synthetic series that comply with the constraints on drought, rainfall intensity, and annual average precipitation depth likelihood. To meet both drought and total precipitation depth constraints, discrete events were incorporated to the WG formulation in Martin (2023) to provide for infrequent extreme precipitation events that allowed the calibrated WG to jointly adhere to the competing constraints.

Table 1 lists the discrete event configurations in the WG formulation and compares them to 24-hour precipitation depths provided by Perica et al. (2018). The 100-year, 24-hour event value of 343 *mm* in Table 1 identifies that the engineering design criteria, related to flooding with a 1% annual probability of exceedance, increased by 1.5 times ($343 \text{ mm} / 233.7 \text{ mm} = 1.5$) after the bridge and the 44 houses were designed and constructed. Note that the discrete event formulation described in Table 1 provides for a possible magnitude of up to 498 *mm* for the discrete event with an average recurrence interval of 100 years.

The initiating event in Figure 4 is a daily precipitation depth that is greater than or equal to 236 *mm* (9.3 *in*). Each weather realization is queried for individual days with simulated precipitation depth meeting the initiating event criterion. When an initiating event is found, flood water surface elevation and foundation inundation depth are determined by simulating the event as discussed in Section 2.3. There are 3,583 daily

events with precipitation depth exceeding 236 mm across the 1,000 synthetic future weather realizations. Figure 6 shows the distribution of number of initiating events within realizations and the likelihood per initiating event depth value.

2.2.1 Stationarity

Engineering uncertainty, see Figure 1, is analyzed under the assumption of a fixed and known “target”. A fixed target requires assumption of time stationarity, which means that statistical properties (and statistical moments) of a series be invariant with time. A relaxed form of stationarity, called weak stationarity, is often used for the analysis of water resource observations. It requires a constant mean and an autocovariance function that depends only on the time difference, or lag, and is independent of the points in time that are differenced (Cryer and Chan, 2008; Shumway and Stoffer, 2017). Weak stationarity only involves the first two statistical moments.

When traditional engineering-style extreme value, frequency analysis is implemented, a probability distribution is used to describe event recurrence interval and magnitude (World Meteorological Organization, 2009). A symmetrical distribution shape, like provided by the Gaussian or normal distribution, requires assumption of weak stationarity because unique values for the mean (which is the first statistical moment) and variance (which is the second statistical moment) are required to define the distribution. Non-symmetrical distribution shapes, like Weibull and Generalized Extreme Event (GEV) distributions, are typically used to represent extremes because it is expected that distribution shape will be skewed towards smaller values. Probability distributions with non-symmetrical shapes require assumption of strict stationarity because unique parameter values are required for at least the first three statistical moments to define a distribution with a non-symmetrical shape.

Figure S1 from Martin (2023) shows three data sets that are not stationary relative to each other because each provides a different likelihood for a given weather magnitude. The “SPEI from WG 2031–2060” option in Panel (c) is the synthetic daily weather data set used to determine initiating event occurrence. Note that stationarity is assumed within each data set in order to calculate the Standardized Precipitation Evapotranspiration Index (SPEI) because this calculation requires definition of a non-symmetrical probability distribution. Data sufficiency considerations require that the 2N recurrence interval event is the maximum recurrence interval that can be estimated based on N years of data (World Meteorological Organization, 2009). Consequently, the “SPEI from WG 2031–2060” data set can only estimate to the 1.67% ($= 1 / (2 \times 30)$) annual probability of exceedance.

Backward looking engineering uncertainty analyses are especially problematic when applied to evaluate highly variable data sets like weather and climate. History provides a single realization of weather, which is unlikely to include the full range of extremes that could be produced given a known range of atmospheric, oceanic, and near-earth surface and soil conditions, from which to deduce a climate description (Fowler et al., 2024; Martin, 2021b). For example, there is not currently an accepted proof of the existence of an upper bound on possible rainfall, i.e., a probable maximum precipitation (PMP) value. PMP values are estimated based on limited historical observations and have been exceeded by observations subsequent to the PMP calculation (National Academies of Sciences, Engineering, and Medicine, 2024).

Although the WG-produced synthetic weather series include an assumption of stationarity across 2024–2065, the goal for the WG constraint, and calibration, is to produce sufficient variability (or variance in values) to compensate for the planning uncertainty inherent in a cone of uncertainty, see Figure 3. Conceptually, this goal is the attempt to include sufficient variability to cover estimated planning uncertainty at the future end of the cone and to hold this amount of variability constant from the present

through the end of the cone of uncertainty as shown on Figure 7. Holding the variance approximately constant across 2024–2065 will result in approximately constant percentile values (i.e., flat lines) and constant uncertainty envelope width (Martin, 2021b,a), as shown on Figure 7, in contrast to the standard cone of uncertainty representation that has an increasing mean and variance trend with time.

2.3 Inundation Simulation

The study site configuration shown on Figure 5 was designed so that increased inflow discharge will produce a greater degree of flood inundation. The relative channel constriction created by the bridge downstream of the houses ensures that the original design basis event, i.e., an inflow discharge of $180 \text{ m}^3/\text{s}$ corresponding to a daily precipitation depth of 236 mm , passes through the channel constriction without flooding any houses. As the inflow discharge increases above $180 \text{ m}^3/\text{s}$ then flood inundation becomes possible because of the conveyance capacity limitation of the bridge opening.

To simulate inundation at the study site, a numerical model must represent: 1) a free surface and 2) conservation of momentum. The combined free surface and conservation of momentum representation allows for determination of backwater effects and of increased water depth with partial blockage as momentum is conserved and flow velocity, i.e., kinematic energy, is transformed to water depth, i.e., potential energy, as incompressible water piles up behind the blockage. The MOD_FreeSurf2D model is used to simulate inundation at the study site. It is an open-source and freely available research tool for simulating fluid flow and rivers and streams which provides a combined free surface and conservation of momentum representation (Martin and Gorelick, 2005).

MOD_FreeSurf2D is the Matlab-based implementation of the semi-implicit, semi-Lagrangian finite-volume approximation to the depth-averaged shallow water equations of Casulli and Cheng (1992) and related work (Casulli, 1990; Casulli and Cattani, 1994; Casulli, 1998, 1999). This is mature, and maybe even legacy, technology from the 1980s and 1990s. The Matlab implementation allows use of well tested and optimized mathematical libraries, i.e., from Matlab, for combining the mature and elegant numerical methods created and documented by Casulli (1990); Casulli and Cheng (1992); Casulli and Cattani (1994); Casulli (1998, 1999). Martin and Gorelick (2005) provide summary of the MOD_FreeSurf2D implementation of these numerical methods and provide dam-break and river flow validation experiments.

A strength of MOD_FreeSurf2D for the study site is the transparent handling of wetting and drying. Channel boundaries within the simulation domain do not require specification, as the model automatically determines wetting or drying in response to any change in flow conditions. Consequently, the model naturally finds the amount of inundation based on topography for small rivers and streams and based on bathymetry for estuaries, reservoirs, and large rivers. The Tidal, Residual, Intertidal Mudflat (TRIM) Model originally presented this efficient solution for wetting and drying, along with the semi-implicit, semi-Lagrangian finite-volume algorithm of Casulli and Cheng (1992), and was used to successfully simulate tidal currents, tidal driven wetting and drying, and baroclinic forcing for San Francisco Bay in the early 1990s (Cheng et al., 1993).

A fundamental limitation for simulation of flooding considerations with MOD_FreeSurf2D is that it will over-estimate fluid velocities because it portrays the depth-averaged shallow water equations and is essentially two-dimensional (2D). A 2D representation will over-estimate flood velocity because of the lack of a vertical dimension, which would allow vertical velocity to contribute to water piling up behind an obstruction, and a sub-grid turbulence closure, which would provide for velocity decay within the water column. This limitation is presented and discussed in the “Application I: Flume experiment dam-break case” of Martin and Gorelick (2005).

2.3.1 MOD_FreeSurf2D Implementation

For the study site, MOD_FreeSurf2D requires specification of: 1) volumetric inflow discharge by boundary grid cell, 2) topographic elevations across the domain on a regular grid, 3) initial water depths, which can be zero, across the domain on a regular grid, 4) Manning's roughness coefficient for each cell in the regular grid, and 5) outflow radiation boundary condition type by boundary grid cell. Each simulation has a duration of six hours and uses a two second time step. The regular grid is 200 rows by 70 columns of 5 m by 5 m cells.

Inflow discharge is determined by multiplying projected daily precipitation depth by the scaling factor of $180.0 \text{ m}^3/\text{s}$ per 236 mm, as discussed in Section 2.1. Topographic elevations are shown on Figure 5. Cells that are within a "house" footprint are set to an elevation of 120.0 m so that water has to flow around, and not through, the house for determination of flood water surface elevations. The bridge in Figure 5 is only represented with topographic elevations for ground surface; a bridge deck is not included in the representation. The initial water depths are not critical for obtaining a solution. A "good" initial depth value is anything between zero and a reasonable estimate for the normal water depth for each grid cell location at the onset of flooding. A Manning's roughness coefficient, or Manning's N , value of $0.040 \text{ s/m}^{1/3}$ is and the radiation free surface outflow boundary condition of Orlanski (1976) are used for all pertinent cells and simulations.

Figure S2 displays water surface elevations simulated using MOD_FreeSurf2D for the historical design event case on Panel (a) and for the current design event case on Panel (b). The historical design event simulation shows compliance and thus no simulated water elevations above foundation elevations. For the current design event shown on Panel (b), there is simulated flooding of 16 houses with a maximum foundation inundation depth of 2 m for House #33.

2.4 Obstruction Representation

The "obstruction" event on Figure 4 provides for inclusion of a stochastic obstruction height as part of the "Stochastic Obstruction Height" branch. All 3,583 daily precipitation events are simulated with an obstruction depth of zero on the "No Obstruction" branch and with an obstruction depth randomly sampled from the Generalized Extreme Value (GEV) distribution shown on Figure 8 as part of the "Stochastic Obstruction Height" branch. Consequently, system failure is evaluated 7,166 times to determine overall failure likelihood.

"Obstruction height" is a conceptualization of the possible degree of channel blockage by debris, transported during the flood event, that is caught in the bridge opening. All events simulated in this study exceed the historical 100-year recurrence event magnitude, which was applicable at the time of design; consequently, it is reasonable to expect the possibility for entrainment of trees, debris, and maybe even structures at these high flood stages and to expect the possibility for debris blockage of the relatively constricted bridge opening. Sampled obstruction height is added to the undisturbed topographic elevation for the two "Obstruction Locations" shown on Figure 5 Panel (b) to increase the topographic elevation seen by the model to undisturbed topographic elevation plus obstruction height. This sum is limited to a maximum elevation value of 105.033 m which is the elevation for the road surface and which corresponds to a maximum obstruction height of 13.333 m.

The GEV distribution, shown on Figure 8 with the "Theoretical Obstruction" lines, was created so that obstruction height would be less than or equal to 1.0 m for about 50% of samples. It provides a theoretical formulation because it is defined using closed form equations for the cumulative distribution function

(CDF) and probability density function (PDF). The particular GEV instance shown is obtained by selecting values for three parameters: shape ($= -0.3$), scale ($= 1.0$), and location ($= 0.62$). For the selected GEV instance, cumulative probability for an obstruction height of 1 m is 0.498 , is 0.989 for 10 m , and is 0.995 for 13.333 m .

An obstruction height is sampled for the “Stochastic Obstruction Height” branch, and obstruction height is fixed to zero for the “No Obstruction” branch of the event tree. When the distribution of obstruction depths across both branches is examined, the empirical or sampled distribution of obstruction height will be normalized to include that half of evaluations that use an obstruction height of zero. The result is the “Empirical Obstruction CDF” shown on Figure 8 Panel (a) and the “Sampled Obstruction PMF” on Figure 8 Panel (b). The probability mass function (PMF) is the normalized histogram of the obstruction heights used across both branches, and a PMF is the discrete and empirical analog to the continuous theoretical PDF.

Figure S3 provides examples of the impact of obstruction height to simulated water surface elevation. Panel (a) shows that an obstruction height of about 5.1 m will cause flooding damage for the historical design basis event; however, note that accounting for possible obstruction was not part of the historical design requirements. Panel (b) displays the maximum water surface elevation simulated in the $7,166$ evaluations. In Figure S3, the application of the obstruction height to the “Obstruction Locations”, shown on Figure 5 Panel (b), is evident from the relatively shallow water depths at these locations.

2.5 Damage Cost Estimation

Paulik et al. (2022) found that total building damage is strongly correlated to flood inundation depth above the first finished floor elevation and that flow velocity is important for determining structure component damage. Component damage refers to which parts of the building, like internal finishes, are damaged. Peña et al. (2023) use simulated inundation depth and the Delft Flood Impact Assessment Tool (Delft-FIAT) (Slager et al., 2016) to calculate flood damage for the Arch Creek Basin in Florida. This tool uses water depth and user specified depth-damage curves as inputs to evaluate damages per asset where assets include buildings roads, utilities, etc.

In this study, we use a simple estimation of damage cost by inundation depth rather than both inundation depth and velocity magnitude to keep the analysis as simple as possible because the study site is synthetic and to avoid the velocity estimation limitations of 2D models, discussed in Section 2.3. We develop a single inundation depth-damage curve for the houses. The damage curve is applied to estimate cost as part of the PRA without using external tools. Flood inundation assessment is generated using inputs from two precursor events in the event tree: 1) inflow discharge and 2) topographic elevations at the “Obstruction Locations” in Figure 5 Panel (b).

Figure 9 shows the damage cost curve used to attribute value of damage based on inundation depth. This curve was derived using damage cost estimates by inundation depth from the Federal Emergency Management Administration (FEMA) National Flood Insurance Program (NFIP) online Flood Damage Cost Calculator (accessed on 3 September 2024) for a 464.5 m^2 ($5,000\text{ ft}^2$), two-story house. The Flood Damage Cost Calculator provides damage cost estimates for inundation up to 1.219 m (48 in). Damage estimates for inundation depths larger than 1.219 m were determined using linear interpolation between 1.219 m and the assumed “Complete Loss” depth of 2.743 m (108 in). Based on the most recent average real estate values across urban areas and coastal regions across the US, it is assumed that the total value, corresponding to “Complete Loss”, for each house is $\$750,000$ (National Association of Realtors, 2024).

3 RESULTS

System failure is occurrence of a “damage to compliant residence” event in Figure 4. Magnitude of damage is cast to cost using the curve shown on Figure 9. There may be zero to ten initiating events within a weather realization per Figure 6. The total number of initiating events for the ensemble of 1,000 weather realizations is 3,583, and the damage costs resulting from each initiating event, within a realization, are summed to determine a realization total cost.

Each future weather realization covers 2024–2065 (for this study). The ensemble of future weather realizations provides a probabilistic climate description. Note that each initiating event is evaluated twice because of the “obstruction” event in Figure 4. One evaluation occurs for the “No Obstruction” branch using an obstruction height of 0.0 *m*, and one occurs for the “Stochastic Obstruction Height” branch using an obstruction height sampled from the theoretical GEV distribution shown on Figure 8. As a result, there are 7,166 failure evaluations from 3,583 initiating events.

The results, and risks, are likelihood of total damage cost across 2024–2065. Figure 10 displays the cumulative distribution functions (CDFs) for estimated total cost across the ensemble of 1,000 future weather realizations. “All Failures” depict the averaged total cost across both “obstruction” event branches in Figure 4. Total averaged cost for a future weather realization is determined because each initiating event is evaluated twice. “No Obstruction” provides the likelihood of total cost from the obstruction depth fixed to zero branch, and “Obstruction Only” displays cumulative probability of total cost from the “Stochastic Obstruction Height” branch.

In Figure 10, the largest relative cost increase from inclusion of channel obstruction occurs between 60 and 80% likelihood. The daily precipitation depth range for 60 and 80% likelihood is approximately 262 to 303 *mm* from Figure 6 Panel (b). This range provides inflow discharge that can generate minor flooding of two or more houses without factoring in the possibilities for channel obstruction, see Figure S1. When the possibility for channel obstruction is included in the analysis, then any amount of obstruction, combined with inflow discharges in this range, will contribute to relatively increased depth of inundation and thus increased damage estimates.

The site geometry, shown on Figure 5, creates an environment where the houses closest to the bridge and to the channel center line are most likely to flood. Figure 11 provides the proportion of initiating events that result in damage to each house. The two houses closest to both the bridge and channel are House #22 and #33, which are damaged in over 35% of the events evaluated. Houses #12 and #23 are farthest from the bridge and are only damaged in about 12% of evaluated events.

Table 2 presents likelihood of total cost estimates for the scenarios presented on Figure 10 and for the additional “Drop 4 Houses”, “Drop 6 Houses”, “Drop 8 Houses”, “Drop 12 Houses”, “Drop 14 Houses”, “Drop 16 Houses”, and “Drop 18 Houses” scenarios. This table shows the same divergence in total estimated damage costs across the scenarios above 60% cumulative probability as shown on Figure 10. The purpose of the “Drop Houses” scenarios is to examine conceptually when it might save money overall to remove houses in the near future to avoid repeated damage costs across 2024–2065.

For the “Drop 2 Houses” scenario examined on Figure 10, Houses #22 and #33 are the two houses dropped from the analysis because these are the two houses most likely to flood. The next two most likely houses to flood are Houses #21 and #32, which are immediately upstream of #22 and #33 in the line of houses closest to the channel on each bank. The “Drop 10 Houses” scenario, shown on Figure 11, is the removal of the five houses closest to the bridge from the line of houses closest to the channel on each bank

from damage cost estimations (the houses removed are #22, #21, #20, #19, and #18 from the left bank and #33, #32, #31, #30, and #29 from the right bank). Similarly, the houses dropped from damage cost calculations for the “Drop 18 Houses” scenario are #22, #21, #20, #19, #18, #17, #16, #15 and #14 from the left bank and #33, #32, #31, #30, #29, #28, #27, #26 and #25 from the right bank. These are the 18 most likely houses to be damaged as shown on Figure 11.

Table 3 provides estimated cost savings for the likelihoods, or percentiles, shown on Table 2. Cost Savings Relative to “All Failures” on Table 3 is calculated from Table 2 as the “All Failures” value less the sum of the “Drop Houses” scenario value and the corresponding “House Removal” cost. For example, the 90th Percentile, \$1.0 M cost savings for the “Drop 4 Houses” scenarios is determined by subtracting the sum of the 90th Percentile “Drop 4 Houses” value and “House Removal Cost” for removing four houses from the 90th Percentile “All Failures” value ($1.045 = 17.099 - (13.054 + 3.0)$).

In Table 3, total cost savings are projected at the 75th percentile level for “Drop 2 Houses”, “Drop 4 Houses”, “Drop 6 Houses”, “Drop 8 Houses”, and “Drop 10 Houses” scenarios with the maximum cost savings of \$0.6M estimated for the “Drop 6 Houses” scenario. All “Drop Houses” scenarios provide estimated cost savings at the 90th percentile and maximum cost (maximum cost is the 100th percentile) levels. Maximum cost savings of \$1.6M is estimated for the “Drop 16 Houses” scenario at the 90th percentile level and of \$34.9M for the “Drop 18 Houses” scenario at the 100th percentile level.

4 DISCUSSION

This paper presents an approach to optimizing resource use, given a present environment of unplanned for rapidly changing climate, so that future generations can safely meet their needs. Sustainability enters the analysis through decision making based on Table 3. Specifically, the percentile used for decision making determines the desired degree of sustainability and use of the “Max”, or 100th percentile, column in Table 3 provides the most weight towards the ability of future generations to meet their needs. As mentioned previously, the “Drop 18 Houses” scenario provides the most cost savings, of the examined scenarios, for the 100th percentile damage costs. In Table 2, the “Max” total cost for the “Drop 18 Houses” scenario is approximately \$7M, which is approximately equivalent to the “All Failures” mean cost of \$7M. This means that future generations can expect the same degree of damage from the “Drop 18 Houses” scenario under the worst conditions as from the “All Failures”, or existing conditions, scenario under “expected”, or average, future climate with the additional cost of removing 18 houses (\$13.5M).

Rapidly changing climate is largely unplanned for because of the backward looking nature of engineering design bases. Engineering uncertainty relies on the assumption that the “target” value is relatively well, but not exactly, known, and it explicitly assumes that everything observed in the future will be similar to what has already been observed in the past. This is the assumption that allows the labeling of 100-year and 500-year events and that generates surprise when two 500-year events, attributed based on solely historical observations, occur in successive months. History provides but one realization of weather from which to deduce a climate description. For highly variable quantities, like weather, a single realization is a paltry sample of the daily weather that could be generated from any set of combined atmospheric, biospheric, soil moisture, polar ice pack, and oceanic conditions. Consequently, it is poor decision support to assume that future conditions will never exceed the boundaries provided by recent history.

In Table 1, the Perica et al. (2018) 100-year recurrence precipitation depth of 343 mm is 1.5 times larger than the historical design basis from Hershfield (1963). The constrained WG uniform distribution, upper bound estimate is 498 mm, or about 2.1 times larger than the historical basis event, and the lower bound

estimate is fixed to 343 *mm*. Each time the 100-year, average recurrence discrete event is triggered in the WG, a daily precipitation depth is sampled from the uniform distribution and thus selected from the range 343 to 498 *mm*. Consequently, the synthetic weather series are non-stationary with both current and historical climate. From the empirical CDF on Figure 6 (b), a precipitation depth of 343 *mm* has a cumulative probability of 0.866, and a depth of 498 *mm* has a cumulative probability of 0.991.

The collection of precipitation depths, shown on Figure 6, is an extraction from 1,000, 42-year duration daily time series and is not a complete duration annual maximum series. A complete duration annual maximum series is required to estimate recurrence interval, in years, under the assumption that there is only one major precipitation event (and not multiple similar events or even no events at all) during every year in the series. Even if we desired to make a traditional (and misguided) estimate of recurrence interval, the maximum recurrence interval that could be estimated from the probabilistic climate ensemble is the one in 84-year, average recurrence event because there are only 42 years in the data set ($N = 42$ and $2N = 84$) (World Meteorological Organization, 2009).

It does not matter which computer model is used to estimate water surface elevation based on inflow discharge and topography in this analysis as long as it meets the basic requirements of a combined free surface and conservation of momentum representation. MOD_FreeSurf2D was used because it was accessible to the authors, it is mature technology, and it will run on a laptop for a simulation domain of the size shown on Figure 5 Panel (a). The style of model needed for this study solves a boundary value problem using a system of partial differential equations (PDEs) across a computational mesh that discretizes the interior of the solution domain.

For boundary value problems, boundary forcing and boundary specification have first order control over the PDE solution. Parameters, like Manning's N , have at best a second order impact to the PDE solution. The most important component for this analysis is the observed 1.5 times increase in the primary design basis between 1963 and 2018. This expectation for large increase in inflow discharge, i.e., boundary forcing, will and does overwhelm all domain interior and numerical model computational parameter considerations. Consequently, parameters like Manning's N , time integration duration (or time step), and Θ degree of implicitness are not varied as part of this analysis. Variations in these parameters will affect model solutions but to a much smaller degree than the primary boundary forcing consideration.

Because many of the evaluations use an inflow discharge specification that is from 1.5 to 2.1 times larger than the historical design basis event, inflow forcing is expected to be the dominant driver of system failure risk. Obstruction height adjusts channel topography, which is a boundary specification. At the maximum value applied to the model, it creates an approximately 13 *m* high embankment or dam. Obstruction height also provides a first order control on likelihood of failure; however, obstruction height is not as significant of a factor as the climate change driven increase in inflow discharge because it only applies to half of the evaluations. The cumulative probability of the maximum obstruction height of 13.333 *m* is 0.995 which only applies to the "Sampled Obstruction Height" half of the evaluations. When this cumulative probability is normalized to represent all evaluations, the cumulative probability is 0.9975, which means that an obstruction height of 13.333 *m* is expected to occur for 0.25% of evaluations.

4.1 Limitations

We have presented a simple and somewhat limited PRA with a single failure scenario. This scenario allows for evaluation of climate change-based flood inundation risk on the existing site configuration, and it provides a template that can be customized for specific sites and real data. However, the event tree, or

527 scenario, specifically applies to the scenario of backward looking engineering uncertainty analyses creating
528 a regulatory compliant land use configuration based on historical, and largely irrelevant, conditions.

529 The event tree on Figure 4 only treats the scenario of clear water inundation. It is possible that future
530 landslides and debris flows could be important property risks and safety considerations. It is also feasible
531 that erosion and material entrainment under house foundations during extreme events could result in whole
532 house entrainment and movement downstream. Erosion, entrainment, and non-Newtonian flows are not
533 explicitly considered. However, a feasible explanation for the maximum obstruction height of 13.333 *m*
534 would be whole house entrainment and wedging of the structure in the bridge opening. “Velocity-based”
535 flood damage is not considered because of inherent limitations of 2D models, which conserve momentum,
536 for accurate velocity prediction.

537 There are also solutions, beyond simple house removal, that are not examined in this analysis. The
538 relative channel constriction provided by the bridge is the limitation on channel capacity that increases
539 flood inundation risk for non-stationary climate. A direct solution would be to replace the existing bridge
540 with a larger one so that there is no channel constriction. The bridge replacement solution could be an
541 attractive approach if the existing bridge is beyond its design life and in need of retrofit.

542 The concept of circularity is related to, but different from, sustainability (U.S. Chamber of Commerce
543 Foundation, 2016). Circularity provides a holistic focus on a complete and closed resource life-cycle where
544 there is not a terminal event involving “disposal” and generation of “waste”. The circular economy is a
545 fairly well known approach that embodies circularity (Ellen Macarthur Foundation, 2024). Regenerative
546 agriculture and “sponge cities” are two holistic natural resources approaches that also embody the concept
547 of circularity. Regenerative agriculture seeks to restore and maintain soil and ecosystem health, address
548 inequity, and leave land, water, and climate in a better shape for the future through focus on how all aspects
549 of agriculture are connected through a fundamentally regenerative web rather than as linear “birth” to
550 “death” supply chain (Natural Resources Defense Council (NRDC), 2021). A “sponge city” is a nature-based
551 solution where urban areas are designed with abundant natural areas including lakes, parks, wetlands, and
552 stream corridors that provide for storm water management through increased infiltration, natural detention,
553 storage, and treatment, and drainage (Hamidi et al., 2021; Harrisberg, 2022).

554 Regenerative agriculture and “sponge cities” are pertinent concepts to this analysis because both seek
555 to increase infiltration, natural detention, and treatment and to reduce fast surface runoff and hazardous
556 flooding. Consequently, regenerative agriculture and “sponge city” planning could contribute to a holistic
557 planning framework that extends the simple design basis planning and flood safety approach of construct
558 now, pay for damage mitigation throughout the development life span, and remove (or worse yet rebuild)
559 facilities as the “terminal” waste event. PRA is fundamentally limited for holistic analysis because it
560 focuses on failure, risk, and consequent cost. Holistic analysis requires balancing contributions from
561 benefits with cost penalties. Probabilistic cost-benefit analysis is the extension to PRA required to support
562 holistic decision making and to examine planning and design that incorporates concepts like regenerative
563 agriculture and “sponge cities”.

564 The important result from this study is not that climate change has increased flooding risk but that
565 suburban and urban development practices based on backward looking engineering uncertainty analyses
566 and design bases are deeply flawed. PRA provides a tool to promote sustainability considerations in any
567 planning or engineering design framework. However, PRA only provides analysis of “costs” from inherent
568 framework risks and does not, in isolation, provide a means to compare benefits with costs.

4.2 Future Work

Examination of PRA utility for sustainable water resources management is implemented at the initial applied research level to minimize implementation costs for exploratory investigation. Table 3 demonstrates that PRA can provide valuable sustainable resources management decision support. Given the possibilities for effective decision support, the next phase of work will be a reach-scale demonstration project using a real site with robust, site-specific data collection.

An adjustment away from regulatory-based protection and defensive measures, based on backward-looking engineering design bases, towards holistic planning approaches that reserve floodplains for water conveyance, storage, and non-development beneficial uses and that eliminate development within the entire feasible flood zone (Mossop, 2021; Kelman, 2020, 2021) is needed to achieve holistic stewardship rather than parsimonious sustainability. As mentioned previously, PRA provides a tool to promote sustainability considerations in planning; however, it has to be extended to include benefit contributions to fully support holistic, flood zone planning approaches. A second component of future work will focus on extending PRA to examine and compare non-development related benefits from, and beneficial uses for, the feasible flood zone in conjunction with risk analysis for existing flood zone development.

CONFLICT OF INTEREST STATEMENT

The authors declare that the research was conducted in the absence of any commercial or financial relationships that could be construed as a potential conflict of interest.

AUTHOR CONTRIBUTIONS

Conceptualization, N.M., ; methodology, N.M.; software, N.M.; writing—original draft preparation, N.M., ; writing—review and editing, N.M., F.P., D.P.; validation, N.M.; funding acquisition, N.M. All authors have read and agreed to the published version of the manuscript.

FUNDING

This study was self-funded by Vodanube, LLC.

ACKNOWLEDGMENTS

This is a short text to acknowledge the contributions of specific colleagues, institutions, or agencies that aided the efforts of the authors. TBD.

SUPPLEMENTAL DATA

Supplementary information, including tables and figures, cited in the main text are available in supplementary materials.

DATA AVAILABILITY STATEMENT

The datasets and source code generated and analyzed for this study can be found in the Future Flood PRA GitHub (accessed 3 December 2024).

REFERENCES

- Alkhatib, S., Sakurahara, T., Reihani, S., Kee, E., Ratte, B., Kaspar, K., et al. (2024). Phenomenological Nondimensional Parameter Decomposition to Enhance the Use of Simulation Modeling in Fire Probabilistic Risk Assessment of Nuclear Power Plants. *Journal of Nuclear Engineering* 5, 226–245. doi:10.3390/jne5030016
- Bernal, G. A., Salgado-Galvez, M. A., Zuloaga, D., Tristancho, J., Gonzalez, D., and Cardona, O.-D. (2017). Integration of Probabilistic and Multi-Hazard Risk Assessment Within Urban Development Planning and Emergency Preparedness and Response: Application to Manizales, Colombia. *International Journal of Disaster Risk Science* 8, 270–283. doi:10.1007/s13753-017-0135-8
- [Dataset] Browne, A. (2022). Explainer: What Is Sustainability and Why Is It Important?
- Casulli, V. (1990). Semi-implicit finite difference methods for the two-dimensional shallow water equations. *Journal of Computational Physics* 86, 56–74. doi:10.1016/0021-9991(90)90091-E
- Casulli, V. (1998). Numerical simulation of three-dimensional free surface flow in isopycnal coordinates. *International Journal for Numerical Methods in Fluids* 25, 645–658. doi:10.1002/(SICI)1097-0363(19970930)25:6<645::AID-FLD579>3.0.CO;2-L
- Casulli, V. (1999). A semi-implicit finite difference method for non-hydrostatic, free-surface flows. *International Journal for Numerical Methods in Fluids* 30, 425–440. doi:10.1002/(SICI)1097-0363(19990630)30:4
- Casulli, V. and Cattani, E. (1994). Stability, accuracy and efficiency of a semi-implicit method for three-dimensional shallow water flow. *Computers & Mathematics with Applications* 27, 99–112. doi:10.1016/0898-1221(94)90059-0
- Casulli, V. and Cheng, R. T. (1992). Semi-implicit finite difference methods for three-dimensional shallow water flow. *International Journal for Numerical Methods in Fluids* 15, 629–648. doi:10.1002/fld.1650150602
- Cheng, R. T., Casulli, V., and Gartner, J. W. (1993). Tidal, Residual, Intertidal Mudflat (TRIM) Model and its Applications to San Francisco Bay, California. *Estuarine, Coastal and Shelf Science* 36, 235–280. doi:10.1006/ecss.1993.1016
- Chow, V. T., Maidment, D. R., and Mays, L. W. (1988). *Applied Hydrology* (McGraw-Hill Education), tata mcgraw edn.
- Clarke, B. and Otto, F. (2023). *Reporting extreme weather and climate change: A guide for journalists*. Tech. rep., world weather attribution (WWA), Imperial College London
- Cryer, J. D. and Chan, K.-S. (2008). *Time Series Analysis with Applications in R*. Springer Texts in Statistics (NY: Springer), second edn.
- [Dataset] Ellen Macarthur Foundation (2024). Circular economy introduction
- [Dataset] Fowler, H. J., Davies, P., and Lee, S. H. (2024). The climate is changing so fast that we haven't seen how bad extreme weather could get
- García-Montiel, E., Zepeda-Mondragón, F., Morones-Esquivel, M. M., Ramírez-Aldaba, H., López-Serrano, P. M., Briseño-Reyes, J., et al. (2023). Probabilistic Risk Assessment of Exposure to Fluoride in Drinking Water in Victoria de Durango, Mexico. *Sustainability* 15, 14630. doi:10.3390/su151914630
- Guadalupe, G. A., Grandez-Yoplac, D. E., Arellanos, E., and Doménech, E. (2024). Probabilistic Risk Assessment of Metals, Acrylamide and Ochratoxin A in Instant Coffee from Brazil, Colombia, Mexico and Peru. *Foods* 13, 726. doi:10.3390/foods13050726
- Hamidi, A., Ramavandi, B., and Sorial, G. A. (2021). Sponge City — An emerging concept in sustainable water resource management: A scientometric analysis. *Resources, Environment and Sustainability* 5, 100028. doi:10.1016/j.resenv.2021.100028

- 640 Han, L., Fan, Y., Chen, R., Zhai, Y., Liu, Z., Zhao, Y., et al. (2023). Probabilistic Risk Assessment of
641 Heavy Metals in Mining Soils Based on Fractions: A Case Study in Southern Shaanxi, China. *Toxics* 11,
642 997. doi:10.3390/toxics11120997
- 643 [Dataset] Harrisberg, K. (2022). What are 'sponge cities' and how can they prevent floods?
- 644 Hershfield, D. M. (1963). *RAINFALL FREQUENCY ATLAS OF THE UNITED STATES for Durations from*
645 *30 Minutes to 24 Hours and Return Periods from 1 to 100 Years*. Technical Report 40, U.S. Department
646 of Commerce, Weather Bureau, Washington, D.C.
- 647 Hsu, F. and Railsback, J. (2004). The Space Shuttle Probabilistic Risk Assessment Framework. In
648 *Probabilistic Safety Assessment and Management*, eds. C. Spitzer, U. Schmocker, and V. N. Dang
649 (London: Springer), 1466–1473. doi:10.1007/978-0-85729-410-4_236
- 650 IPCC (2021). *Climate Change 2021: The Physical Science Basis. Contribution of Working Group I to the*
651 *Sixth Assessment Report of the Intergovernmental Panel on Climate Change* (New York: Cambridge
652 University Press). Doi:10.1017/9781009157896
- 653 Kelman, I. (2020). *Disaster by Choice: How Our Actions Turn Natural Hazard...* (USA: Oxford University
654 Press)
- 655 [Dataset] Kelman, I. (2021). Floods are going to get worse: we need to start preparing for them now
- 656 Kubo, K. (2023). Accident Sequence Precursor Analysis of an Incident in a Japanese Nuclear Power
657 Plant Based on Dynamic Probabilistic Risk Assessment - Kubo - 2023 - Science and Technology of
658 Nuclear Installations - Wiley Online Library. *Science and Technology of Nuclear Installations* 2023, 12.
659 doi:10.1155/2023/7402217
- 660 Landquist, H., Rosén, L., Lindhe, A., and Hassellöv, I.-M. (2016). VRAKA—A Probabilistic Risk
661 Assessment Method for Potentially Polluting Shipwrecks. *Frontiers in Environmental Science* 4.
662 doi:10.3389/fenvs.2016.00049
- 663 Lee, J., Tayfur, H., Hamza, M. M., Alzahrani, Y. A., and Diaconeasa, M. A. (2023). A Limited-Scope
664 Probabilistic Risk Assessment Study to Risk-Inform the Design of a Fuel Storage System for Spent
665 Pebble-Filled Dry Casks. *Eng* 4, 1655–1683. doi:10.3390/eng4020094
- 666 Martin, N. (2021a). Risk Assessment of Future Climate and Land Use/Land Cover Change Impacts on
667 Water Resources. *Hydrology* 8, 1–21. doi:https://doi.org/10.3390/hydrology8010038
- 668 Martin, N. (2021b). Watershed-Scale, Probabilistic Risk Assessment of Water Resources Impacts from
669 Climate Change. *Water* 13, 40. doi:10.3390/w13010040. Number: 1 Publisher: Multidisciplinary Digital
670 Publishing Institute
- 671 Martin, N. (2023). Incorporating Weather Attribution to Future Water Budget Projections. *Hydrology* 10,
672 219. doi:10.3390/hydrology10120219
- 673 Martin, N. and Gorelick, S. M. (2005). MOD_freesurf2d: A MATLAB surface fluid flow model for rivers
674 and streams. *Computers & Geosciences* 31, 929–946. doi:10.1016/j.cageo.2005.03.004
- 675 Martin, N., Nicholaides, K., and Southard, P. (2022). Enhanced Water Resources Risk from Collocation of
676 Disposal Wells and Legacy Oil and Gas Exploration and Production Regions in Texas. *JAWRA Journal*
677 *of the American Water Resources Association* 58, 1433–1453. doi:10.1111/1752-1688.13048. eprint:
678 https://onlinelibrary.wiley.com/doi/pdf/10.1111/1752-1688.13048
- 679 Martin, N. and White, J. (2024). Water Resources' AI–ML Data Uncertainty Risk and Mitigation Using
680 Data Assimilation. *Water* 16. doi:https://doi.org/10.3390/w16192758
- 681 Masoudvaziri, N., Elhami-Khorasani, N., and Sun, K. (2023). Toward Probabilistic Risk Assessment of
682 Wildland–Urban Interface Communities for Wildfires. *Fire Technology* 59, 1379–1403. doi:10.1007/
683 s10694-023-01382-y

- Monge, J. J., Dowling, L. J., Wegner, S., Melia, N., Cheon, P. E. S., Schou, W., et al. (2023). Probabilistic Risk Assessment of the Economy-Wide Impacts From a Changing Wildfire Climate on a Regional Rural Landscape. *Earth's Future* 11, e2022EF003446. doi:10.1029/2022EF003446
- [Dataset] Mossop, E. (2021). Not 'if', but 'when': city planners need to design for flooding. These examples show the way
- National Academies of Sciences, Engineering, and Medicine (2024). *Modernizing Probable Maximum Precipitation Estimation* (Washington, D.C.: National Academies Press). doi:10.17226/27460
- [Dataset] National Association of Realtors (2024). Homes for Sale, Apartments & Houses for Rent
- [Dataset] Natural Resources Defense Council (NRDC) (2021). Regenerative Agriculture 101
- Ololade, I. A., Alabi, B. A., Oladoja, N. A., Ololade, O. O., and Apata, A. O. (2023). Occurrence and probabilistic risk assessment of polycyclic aromatic hydrocarbons in blood and urine of auto-mechanics in Akure Metro, Nigeria. *Environmental Monitoring and Assessment* 195, 727. doi:10.1007/s10661-023-11293-8
- Orlanski, I. (1976). A simple boundary condition for unbounded hyperbolic flows. *Journal of Computational Physics* 21, 251–269. doi:10.1016/0021-9991(76)90023-1
- Pan, X., Ding, S., Zhang, W., Liu, T., Wang, L., and Wang, L. (2022). Probabilistic Risk Assessment in Space Launches Using Bayesian Network with Fuzzy Method. *Aerospace* 9, 311. doi:10.3390/aerospace9060311
- Paulik, R., Wild, A., Zorn, C., and Wotherspoon, L. (2022). Residential building flood damage: Insights on processes and implications for risk assessments. *Journal of Flood Risk Management* 15, e12832. doi:10.1111/jfr3.12832. eprint: <https://onlinelibrary.wiley.com/doi/pdf/10.1111/jfr3.12832>
- Perica, S., Pavlovic, S., St. Laurent, M., Trypaluk, C., Unruh, D., and Wilhite, O. (2018). *NOAA Atlas 14: Precipitation-Frequency Atlas of the United States, Volume 11 Version 2.0: Texas*. Tech. rep., NOAA, Silver Spring, MD
- Peña, F., Obeysekera, J., Jane, R., Nardi, F., Maran, C., Cadogan, A., et al. (2023). Investigating compound flooding in a low elevation coastal karst environment using multivariate statistical and 2D hydrodynamic modeling. *Weather and Climate Extremes* 39, 100534. doi:10.1016/j.wace.2022.100534
- Philip, S., Kew, S., van Oldenborgh, G. J., Otto, F., Vautard, R., van der Wiel, K., et al. (2020). A protocol for probabilistic extreme event attribution analyses. *Advances in Statistical Climatology, Meteorology and Oceanography* 6, 177–203. doi:10.5194/ascmo-6-177-2020
- Rish, W. R. (2005). A probabilistic risk assessment of class I hazardous waste injection wells. In *Developments in Water Science*, eds. C.-F. Tsang and J. A. Apps (Elsevier Science), vol. 52 of *Underground Injection Science and Technology*. 1st edn., 93–135. doi:10.1016/S0167-5648(05)52010-0
- Salgado-Gálvez, M. A., Bernal, G. A., Zuloaga, D., Marulanda, M. C., Cardona, O.-D., and Henao, S. (2017). Probabilistic Seismic Risk Assessment in Manizales, Colombia: Quantifying Losses for Insurance Purposes. *International Journal of Disaster Risk Science* 8, 296–307. doi:10.1007/s13753-017-0137-6
- Sawe, S. F., Shilla, D. A., and Machiwa, J. F. (2021). Assessment of Ecological Risk of Heavy Metals Using Probabilistic Risk Assessment Model (AQUARISK) in Surface Sediments from Wami Estuary, Tanzania. *BioMed Research International* 2021, 6635903. doi:10.1155/2021/6635903
- Schumacher, D. L., Zachariah, M., Otto, F., Barnes, C., Philip, S., Kew, S., et al. (2022). *High temperatures exacerbated by climate change made 2022 Northern Hemisphere soil moisture droughts more likely*. Tech. rep., World Weather Attribution (WWA), Imperial College: London, UK
- Shahsavani, S., Mohammadpour, A., Shooshtarian, M. R., Soleimani, H., Ghalhari, M. R., Badeenezhad, A., et al. (2022). An ontology-based study on water quality: probabilistic risk assessment of exposure

- to fluoride and nitrate in Shiraz drinking water, Iran using fuzzy multi-criteria group decision-making models. *Environmental Monitoring and Assessment* 195, 35. doi:10.1007/s10661-022-10664-x
- Shen, H.-T., Pan, X.-D., and Han, J.-L. (2024). Distribution and Probabilistic Risk Assessment of Antibiotics, Illegal Drugs, and Toxic Elements in Gastropods from Southeast China. *Foods* 13, 1166. doi:10.3390/foods13081166
- Sheng, D., Wen, X., Wu, J., Wu, M., Yu, H., and Zhang, C. (2021). Comprehensive Probabilistic Health Risk Assessment for Exposure to Arsenic and Cadmium in Groundwater. *Environmental Management* 67, 779–792. doi:10.1007/s00267-021-01431-8
- Shumway, R. H. and Stoffer, D. S. (2017). *Time Series Analysis and Its Applications: With R Examples* (Springer), fourth edn.
- [Dataset] Slager, K., Burzel, A., Bos, E., De Bruikn, K., Wagenaar, D., Winsemius, H., et al. (2016). User guide – Delft FIAT
- Stamatelatos, M., Dezfuli, H., Apostolakis, G., Everline, C., Guarro, S., Mathias, D., et al. (2011). *Probabilistic Risk Assessment Procedures Guide for NASA Managers and Practitioners* (Hanover, MD: NASA), second edn.
- Stehle, S., Knäbel, A., and Schulz, R. (2013). Probabilistic risk assessment of insecticide concentrations in agricultural surface waters: a critical appraisal. *Environmental Monitoring and Assessment* 185, 6295–6310. doi:10.1007/s10661-012-3026-x
- [Dataset] United Nations (2024). Sustainability. Publisher: United Nations
- [Dataset] U.S. Chamber of Commerce Foundation (2016). Circularity vs. Sustainability
- van Oldenborgh, G. J., van der Wiel, K., Kew, S., Philip, S., Otto, F., Vautard, R., et al. (2021). Pathways and pitfalls in extreme event attribution. *Climatic Change* 166, 13. doi:10.1007/s10584-021-03071-7
- [Dataset] Vodianube LLC (2024). Uncertainty
- Wang, X., Xia, X., Zhang, X., Gu, X., and Zhang, Q. (2022). Probabilistic Risk Assessment of Soil Slope Stability Subjected to Water Drawdown by Finite Element Limit Analysis. *Applied Sciences* 12, 10282. doi:10.3390/app122010282
- World Meteorological Organization (2009). *Guide to Hydrological Practices, Volume II: Management of Water Resources and Application of Hydrological Practices*, vol. II (Geneva: World Meteorological Organization (WMO)). doi:10.1080/02626667.2011.546602. ISSN: 0262-6667 Publication Title: Guide to Hydrological Practices
- [Dataset] World Weather Attribution (WWA) (2024). Exploring the contribution of climate change to extreme weather events
- Zhao, H., Cheng, Y., Zhang, X., Yu, S., Chen, M., and Zhang, C. (2024). A Probabilistic Statistical Risk Assessment Method for Soil Erosion Using Remote Sensing Data: A Case Study of the Dali River Basin. *Remote Sensing* 16, 3491. doi:10.3390/rs16183491
- Zhou, H., Yue, X., Chen, Y., Liu, Y., and Gong, G. (2023). Comprehensive Environmental and Health Risk Assessment of Soil Heavy Metal(loid)s Considering Uncertainties: The Case of a Typical Metal Mining Area in Daye City, China. *Minerals* 13, 1389. doi:10.3390/min13111389

TABLES

Table 1. Extreme event comparison between NOAA Atlas 14 (Perica et al., 2018) and the weather generator (WG) with events (Martin, 2023).

Recurrence Interval	24-hour Event ¹	WG Event Magnitude Range ²	
(Year)	(mm)	Lower Bound (mm)	Upper Bound (mm)
2	96	96	153.7
5	141	141	247.6
10	179	179	255.7
25	236	236	290.9
50	285	285	415.5
100	343	343	498.1
200	408	NA ³	NA ³
500	506	NA ³	NA ³
1,000	589	NA ³	NA ³

¹ “24-hour event depth” comes from Perica et al. (2018). ² Martin (2023) uses discrete events to represent the extreme events with the recurrence intervals shown. Discrete events are comprised of a Poisson distribution for inter-arrival times, which determine when the event is triggered, and a uniform distribution for event magnitude. “Lower Bound” and “Upper Bound” are the Uniform distribution bounds. WG with discrete events configuration in Martin (2023) provides independent events where more than one event can be triggered for the same wet day. If more than one event is attributed to the same day, the event magnitudes are added to determine the daily precipitation depth. ³ WG with discrete events only uses 2-, 5-, 10-, 25-, 50-, and 100-year events.

Table 2. Comparison of likelihoods for total cost estimates.

Scenario	25 th Percentile	50 th Percentile	Mean	75 th Percentile	90 th Percentile	Max	House Removal ¹
	M\$ ²						
All Failures	0.224	2.461	6.725	11.607	17.099	55.656	NA ³
No Obstruction	0.000	1.272	5.940	10.430	16.193	53.687	NA ³
Obstruction Only	0.325	3.183	7.510	13.590	18.639	57.625	NA ³
Drop 2 Houses	0.025	1.753	5.688	9.818	14.960	48.877	1.5
Drop 4 Houses	0.000	1.104	4.761	8.041	13.054	42.520	3.0
Drop 6 Houses	0.000	0.713	3.944	6.477	11.428	36.705	4.5
Drop 8 Houses	0.000	0.421	3.211	5.030	9.850	31.188	6.0
Drop 10 Houses	0.000	0.173	2.555	3.885	8.251	25.965	7.5
Drop 12 Houses	0.000	0.000	1.964	2.950	6.638	20.972	9.0
Drop 14 Houses	0.000	0.000	1.438	2.038	5.040	16.182	10.5
Drop 16 Houses	0.000	0.000	0.979	1.314	3.504	11.574	12.0
Drop 18 Houses	0.000	0.000	0.588	0.795	2.113	7.251	13.5

¹ “House Removal” provides the total cost for removing the houses as part of the scenario; removal cost is assumed to be the total loss cost of \$750,000. ² “M\$” is million dollars or $\times \$1,000,000$. ³ No houses are removed for the “All”, “No Obstruction”, and “Obstruction Only” scenarios; total cost for removing all 44 houses would be \$33M.

Table 3. Likelihood of cost savings from house removal.

Scenario	Cost Savings Relative to “All Failures” ² (+ is savings and – is extra cost, M\$ ²)					
	25 th Percentile	50 th Percentile	Mean	75 th Percentile	90 th Percentile	Max
Drop 2 Houses	-1.301	-0.792	-0.463	0.289	0.639	5.279
Drop 4 Houses	-2.776	-1.643	-1.035	0.566	1.045	10.136
Drop 6 Houses	-4.276	-2.752	-1.718	0.630	1.171	14.451
Drop 8 Houses	-5.776	-3.960	-2.486	0.577	1.248	18.468
Drop 10 Houses	-7.276	-5.213	-3.329	0.222	1.347	22.191
Drop 12 Houses	-8.776	-6.539	-4.239	-0.343	1.461	25.684
Drop 14 Houses	-10.276	-8.039	-5.213	-0.931	1.558	28.974
Drop 16 Houses	-11.776	-9.539	-6.253	-1.707	1.595	32.082
Drop 18 Houses	-13.276	-11.039	-7.363	-2.688	1.485	34.905

¹ Cost Savings Relative to “All Failures” is calculated from Table 2 as the “All Failures” value less the sum of the “Drop Houses” scenario value and the corresponding “House Removal” cost. ² “M\$” is million dollars or $\times \$1,000,000$.

FIGURE CAPTIONS

- **Accuracy:** how close an attempt is to the center of the target.
 - **Bias:** distance from the average attempt to the center of the target. Also called expected error.
- **Precision:** the spread across all attempts, or how close the attempts are grouped together.
 - **Variance:** expected, or average, distance for all attempts from the average, or expected attempt location.

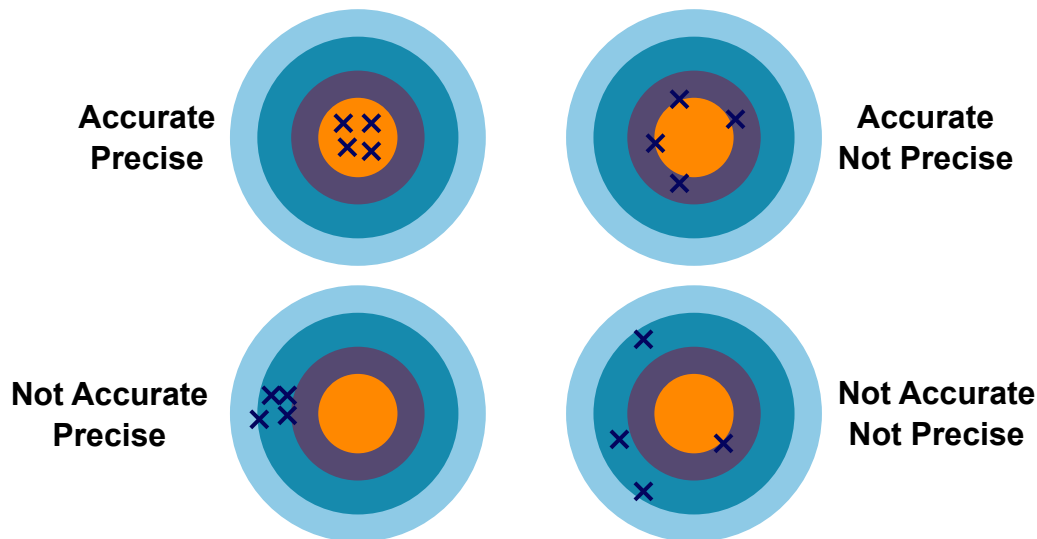


Figure 1. Engineering uncertainty analysis focuses on accuracy and precision relative to design standards. The pre-defined standards provide a target so that can focus on accuracy and precision relative to the target. Bias is the inverse of accuracy, and variance is the inverse of precision. Engineering uncertainty is exact value uncertainty because lack only a high precision delineation of the bullseye. Reproduced from Vodanube LLC (2024). (CC-by-4.0)

- **Truth**: the unknown center of the bullseye. It is unknown because it is not directly observed, but estimated using indirect information.
- **Biased Truth Estimate**: this is the indirect estimate of unknown truth made using calculations based off of other, observed quantities.
- **Extra Variability**: required because "truth" is unknown. The goal for extra variability is to make the target area large enough to include feasible values given inherent uncertainty, but not so large that all attempts are "good" attempts.

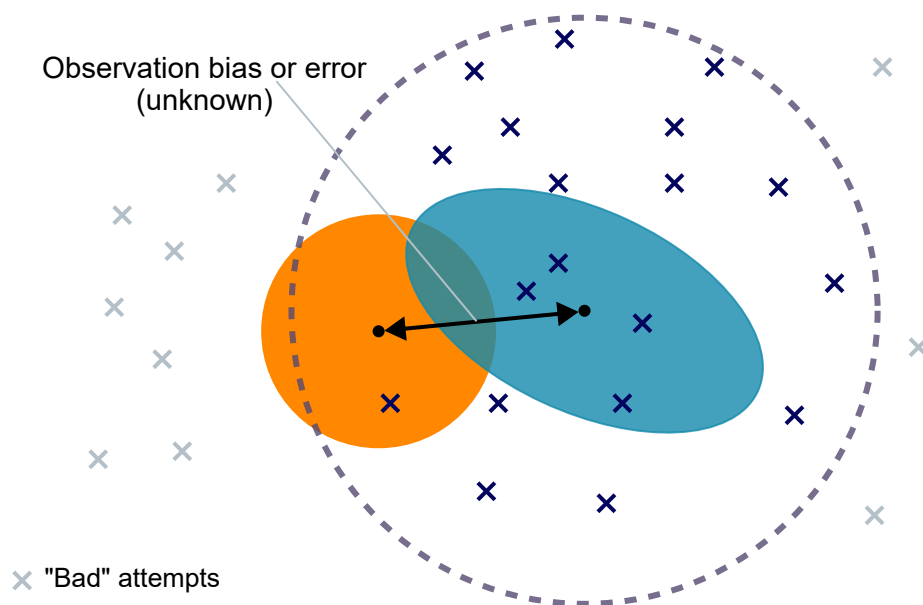


Figure 2. Scientific uncertainty analysis assumes that the true population, or “Truth”, is unknown. Consequently, there is not a well defined “target” as for engineering uncertainty on Figure 1. A “Biased Truth Estimate”, which is biased sample, is available from indirect observations, and the bias comes from observation error as shown on the figure. When a “Biased Truth Estimate” sample is used to constrain the “Truth” population, extra variability is added, denoted by the extent of the “Extra Variability” circle, to attempt to include the “Truth” population within the area of “good” attempts. The location of the “Truth” sample is unknown and extra variability acts to increase the diameter of the “Extra Variability” circle which means that some “good” attempts may actually be worse than some of the “bad” attempts. Reproduced from Vodanube LLC (2024). (CC-by-4.0)

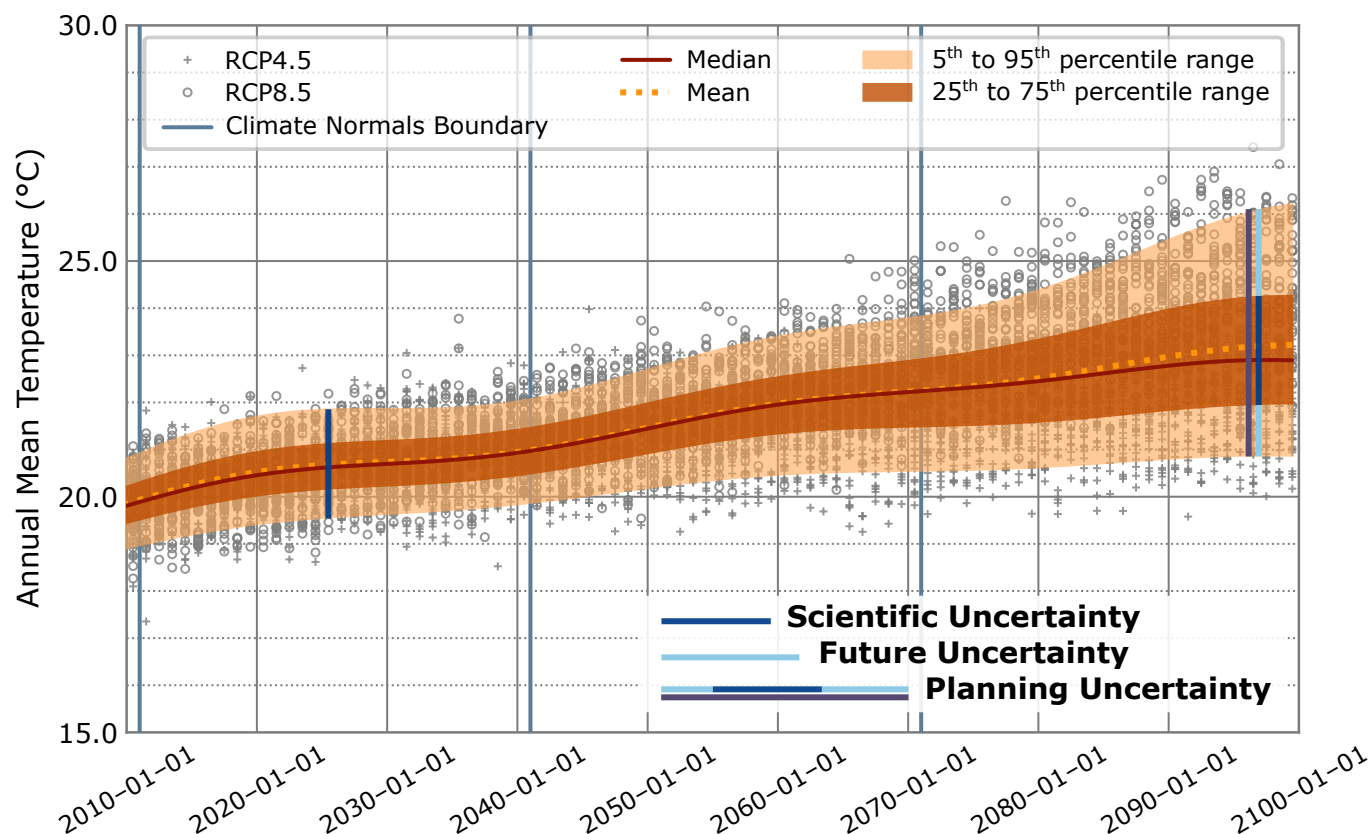


Figure 3. Planning uncertainty sums scientific and future uncertainties. Scientific uncertainty analyses (see Figure 2) attempt to compensate for historical and present day knowledge limitations and observation error with “Extra Variability”. With enhanced variability of estimates, a range of values with corresponding likelihoods (or probabilities) are used to describe certainty and uncertainty. Future conditions are unknown and will likely include environmental conditions outside of what is expected from historical experience. The farther into the future, the greater the amount of uncertainty. The result is a “cone” of uncertainty for future conditions where the cone spreads as uncertainty increases moving into the future, and the cone provides the value and likelihood combinations that are part of scientific uncertainty analysis. The cone of uncertainty shown on this figure is annual mean temperature cone of uncertainty from Coupled Model Intercomparison Project, Phase 5 (CMIP5) Representative Concentration Pathway (RCP) 4.5 and RCP8.5 scenarios. Scientific uncertainty is shown conceptually for approximately present day conditions because it attempts to describe and compensate for historical and present day knowledge limitations with extra variability. In this figure, there is conceptually the same amount of scientific uncertainty in the distant future, i.e., 2095, because it is estimated off of present day and historical conditions, and there is no way to estimate it off of unknown future conditions. Future uncertainty is expected to increase moving forward into the future and thus be larger in the distant future. Planning uncertainty is the total of future uncertainty and scientific uncertainty. Reproduced from Vodanube LLC (2024). (CC-by-4.0)

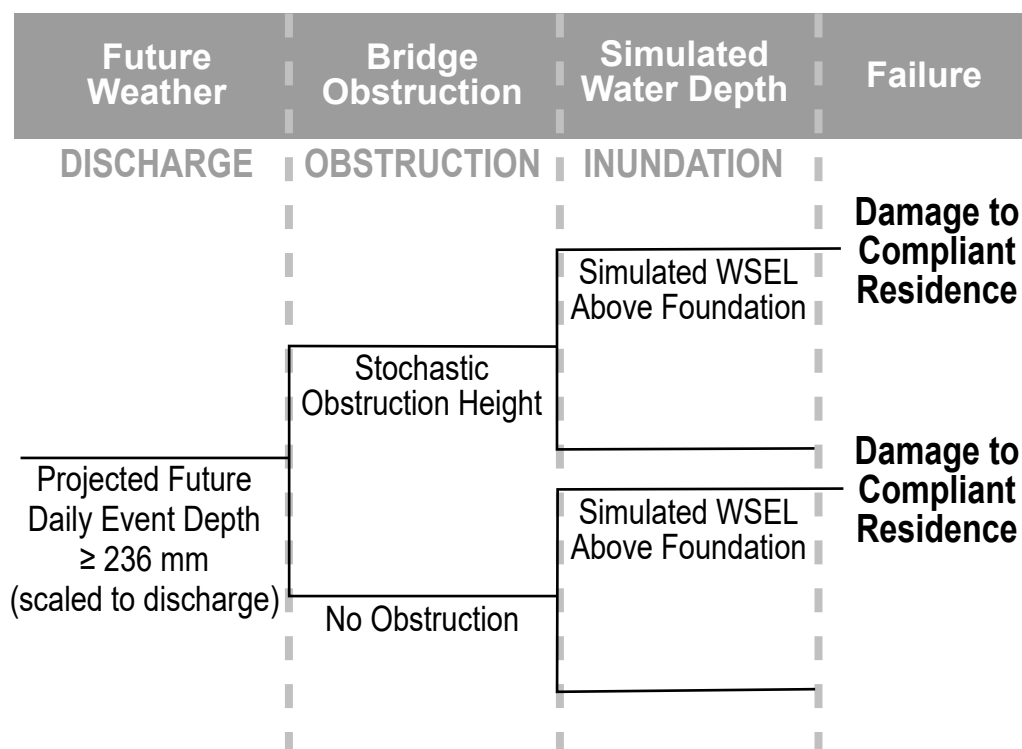


Figure 4. “Precipitation event greater than historical 100-year event” initiating event scenario. This event tree provides the failure scenario evaluated as part of PRA. It is a chain of three events that need to occur for system failure, which is inundation damage to a regulatory-compliant residence. The three events are: 1) “discharge”, “obstruction”, and “inundation”. The “discharge” event occurs when daily precipitation amount exceeds the historical design basis precipitation depth of 233.7 mm and the current 24-hour, 25-year recurrence interval precipitation depth of 236 mm from Perica et al. (2018). The “obstruction” event always occurs, and it is an obstruction height of 0.0 m for the “No Obstruction” branch and a stochastically sampled obstruction height for the “Stochastic Obstruction Height” branch. The “inundation” event is also always evaluated and involves simulation of the water surface elevations (WSEL) at the site using the input specifications of discharge and obstruction height. System failure is simulated WSEL that exceeds foundation elevation for one or more of the 44 houses, see Figure 5.

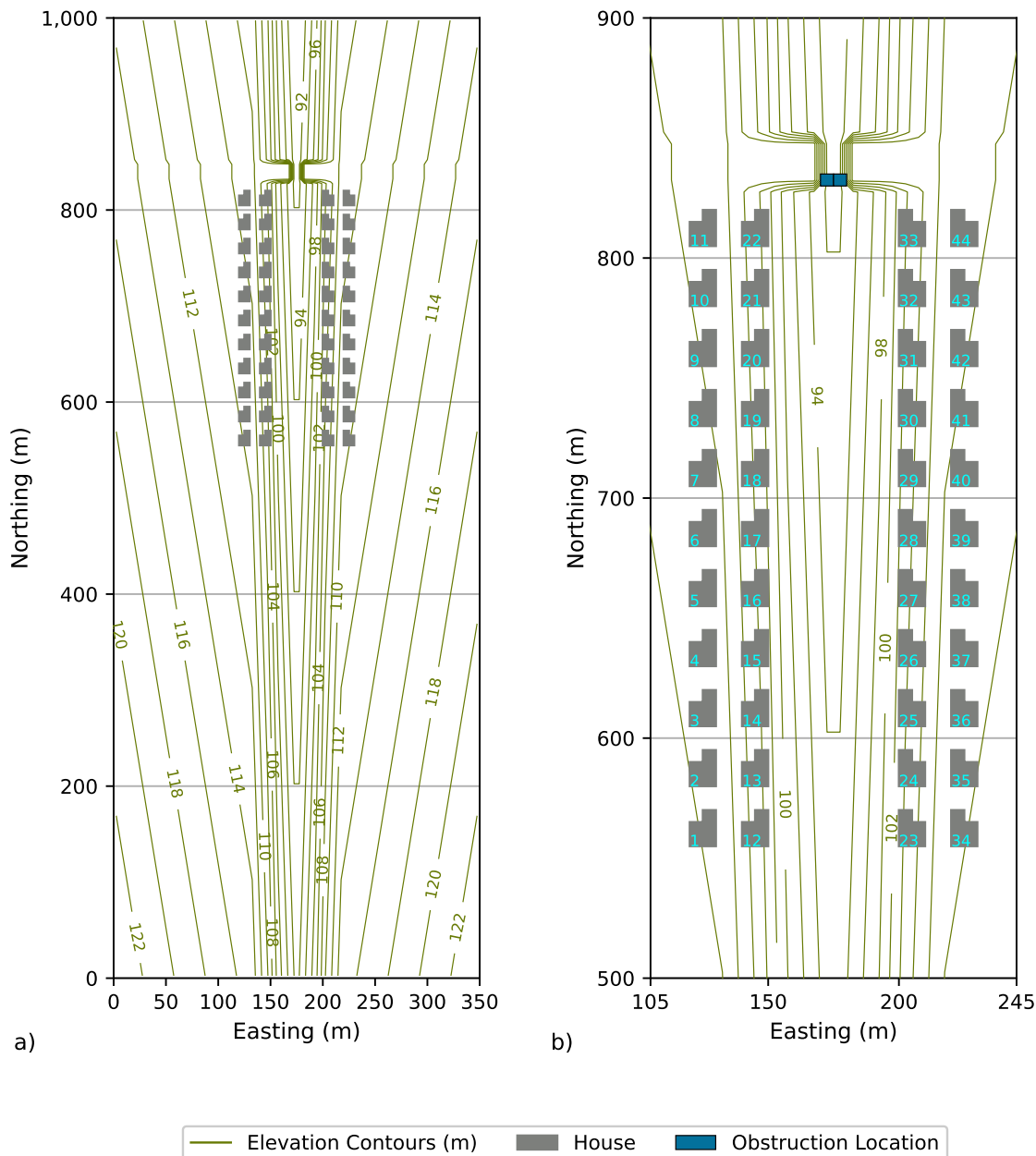


Figure 5. Synthetic site configuration. Panel (a) displays the entire domain, while Panel (b) shows the focus area including the houses and bridge. The two “Obstruction Locations” shown on Panel (b) are the locations where topographic elevation is increased by the sampled obstruction depth. Inflow discharge is applied at 0 m Northing and typically between 150 and 200 m Easting on Panel (a). Radiation-style outflow boundaries are applied at 1,000 m Northing.

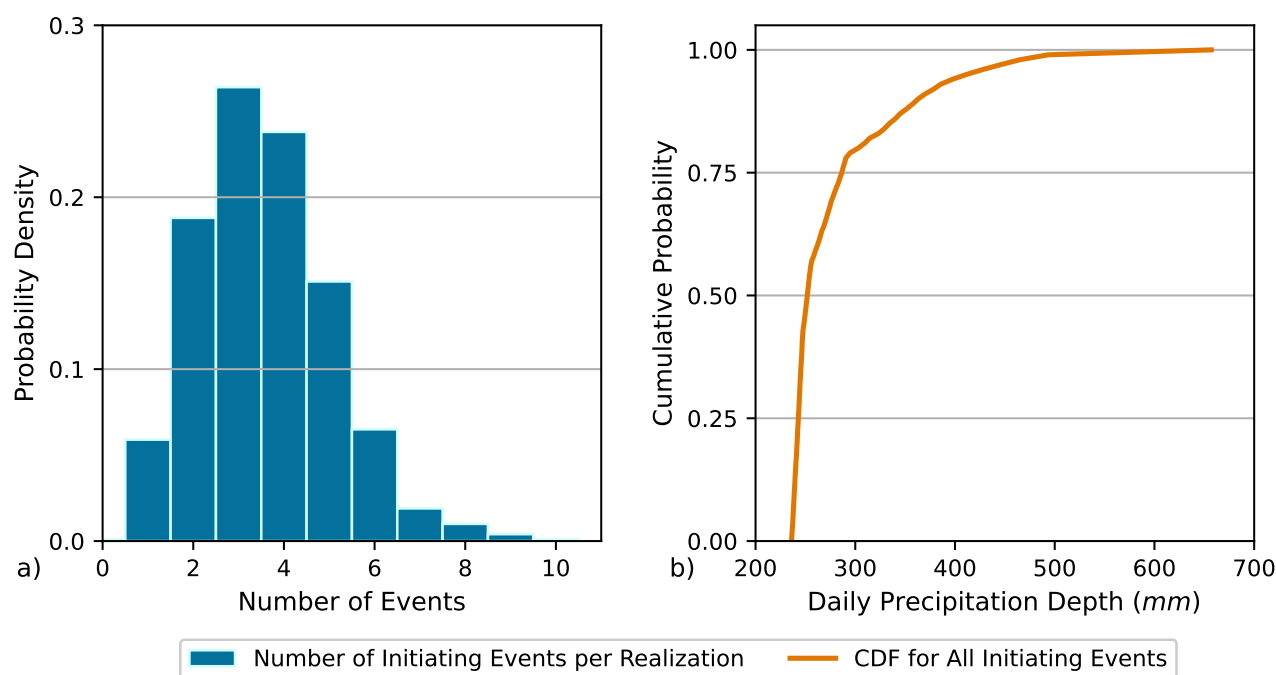


Figure 6. Precipitation event summary across 1,000 future weather realizations covering 2024–2065. Panel (a) identifies the distribution of the number of initiating events that occur within a realization. There is one realization with zero initiating events, and one with 10 initiating events. Panel (b) shows cumulative distribution function for all initiating events across the 1,000 realizations. The minimum initiating event depth is 236 *mm*. Maximum projected daily depth is 657 *mm*.

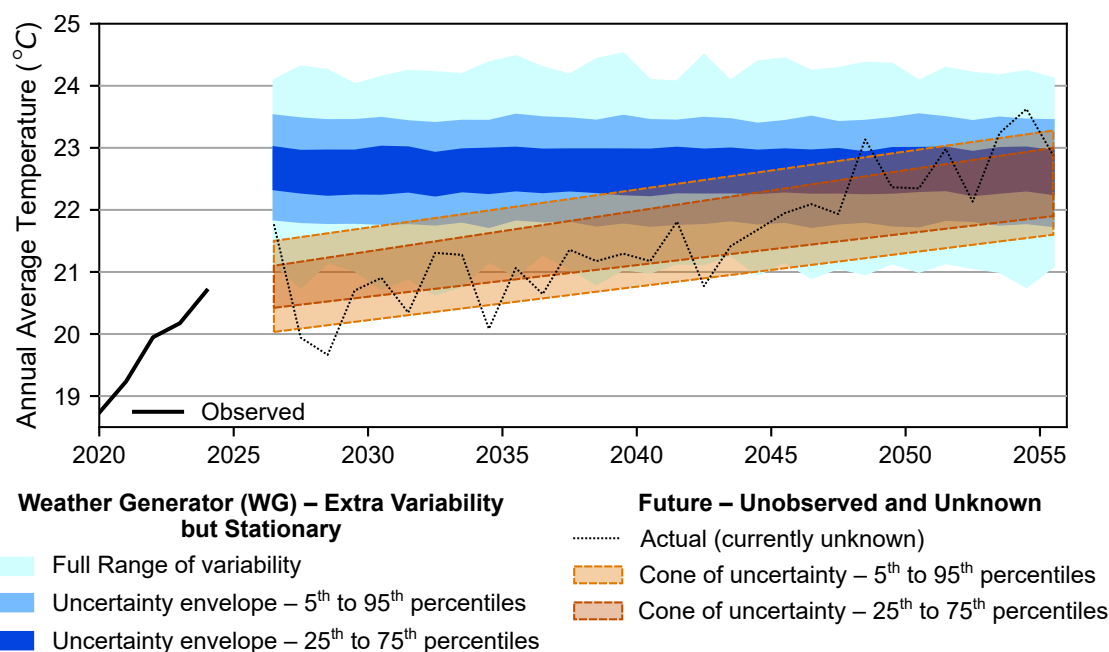


Figure 7. Schematic example of 30-year probabilistic description of expected day-to-day weather variability for temperature. The “Weather Generator (WG) – Extra Variability but Stationary”, i.e., blue shading, presents an example of a 30-year probabilistic description of expected day-to-day weather. The “Future – Unobserved and Unknown”, i.e., orange shading and dotted line, portrays the “unknown” and “true” annual average temperature across this 30-year period (2026–2055 in this example). The “Actual” dotted black line represents the series of temperature values that occur. History provides but one realization of weather from which to deduce a climate description. A single realization is unlikely to depict the full range of extremes that could be produced given a known range of atmospheric, oceanic, and near-earth surface and soil conditions (Fowler et al., 2024; Martin, 2021b). The goal for an ensemble of future weather realizations, which is a probabilistic climate description, is to approximately reproduce the total variability in the future cone of uncertainty, i.e., orange shading, at the target end date in the future. The “Weather Generator (WG) – Extra Variability but Stationary” representation is approximately “flat” denoting lack of trend and time stationarity in the representation.

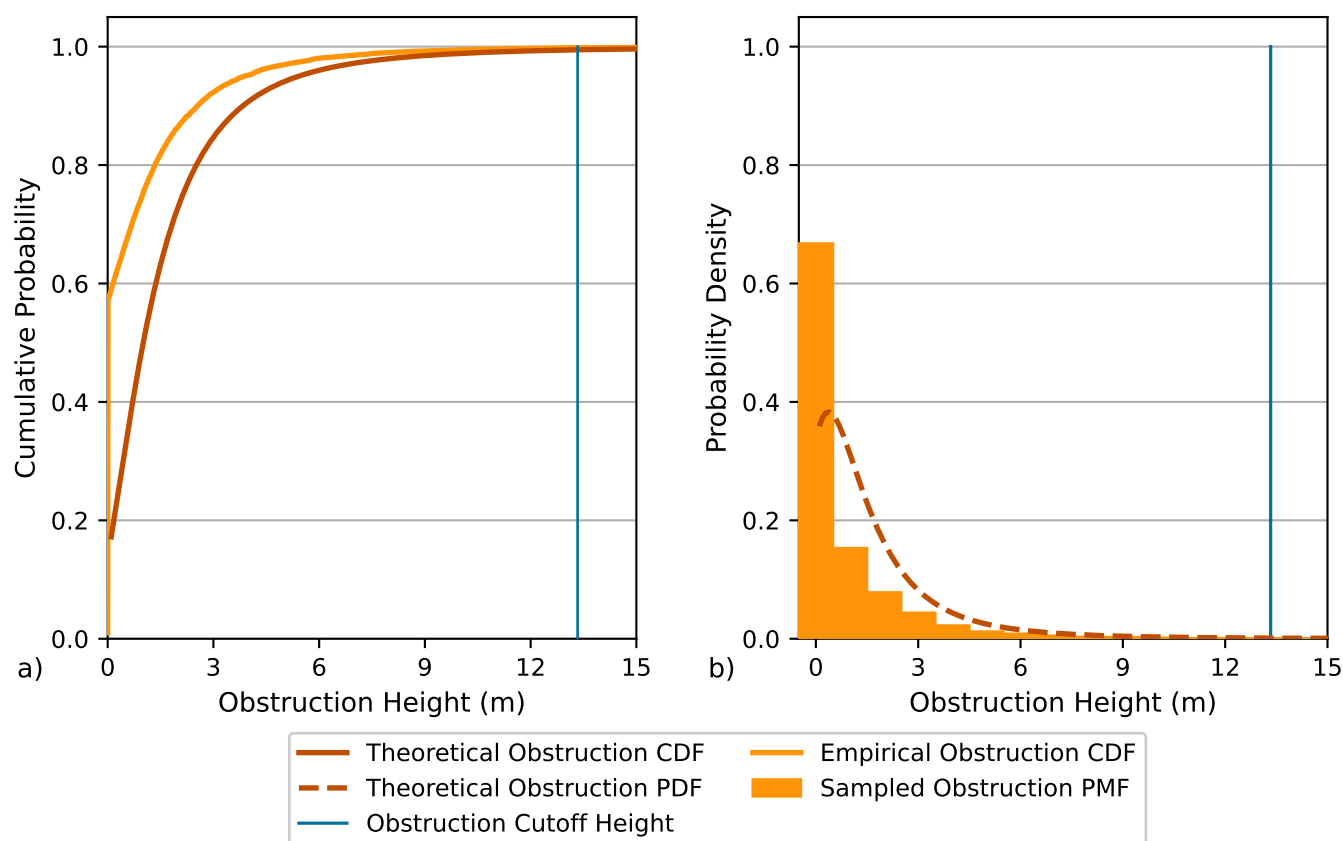


Figure 8. Generalized extreme value (GEV) probability distribution used for sampling obstruction height. This GEV instance is defined using shape = -0.3, scale = 1.0, and location = 0.62. Panel (a) displays the Cumulative Density Function (CDF) of the GEV instance. Cumulative probability for 13.333 m is 0.995 and is 0.498 for 1.0 m. The “Empirical Obstruction CDF” is also shown; it is the cumulative probability distribution of all obstruction heights used across the 7,166 evaluations. Note that half of evaluations (i.e., the “No Obstruction” branch) use an obstruction height of zero, and this is why the “Empirical Obstruction CDF” shows a zero obstruction height for almost 60% of evaluations. Panel (b) shows the Probability Density Function (PDF) for the GEV instance and the “Sampled Obstruction PMF”, which is the normalized histogram of the obstruction heights used across the 7,166 evaluations. PMF stands for Probability Mass Function. The “Obstruction Cutoff Height” is 13.333 m and the maximum obstruction height used with the model because it makes the topographic elevation of an “Obstruction Location”, see Figure 5, equal to the elevation of the road.

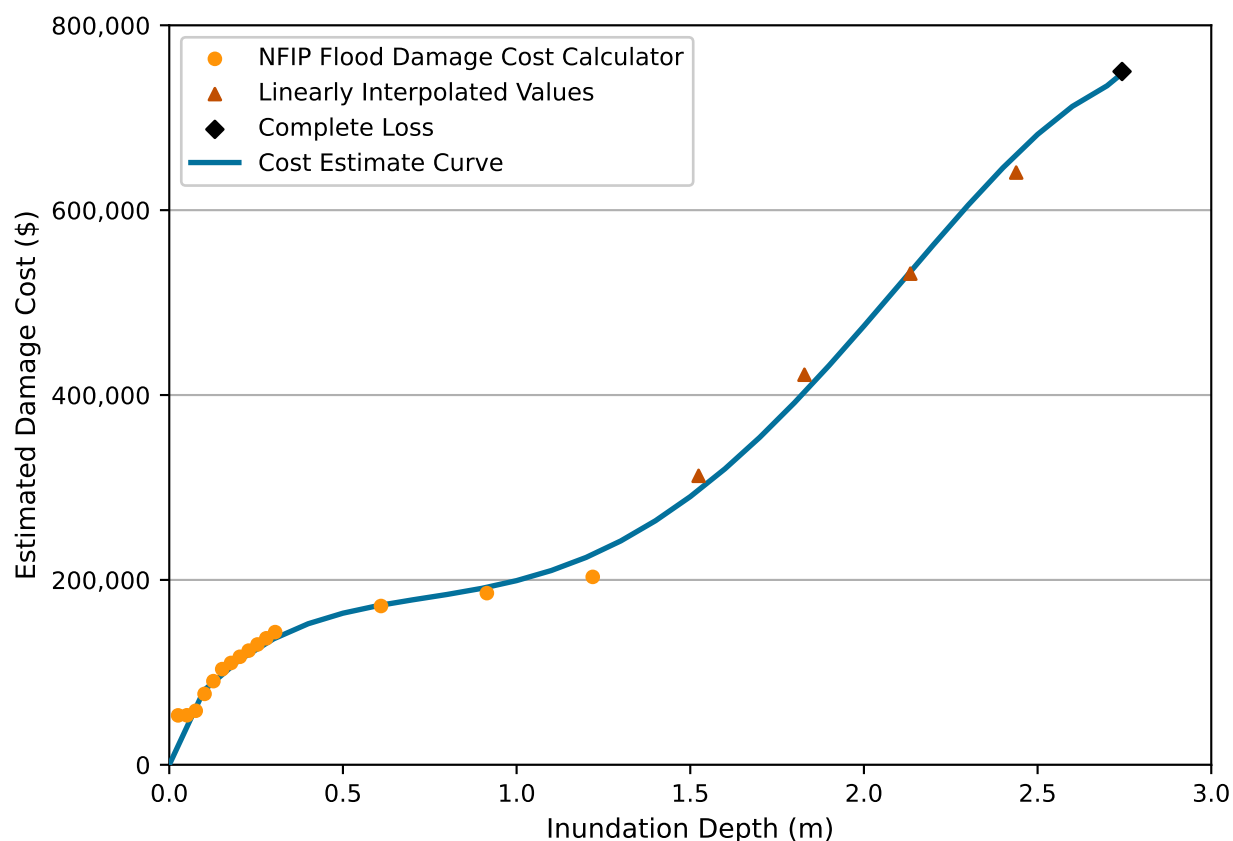


Figure 9. Estimated damage cost curve by inundation depth. The NFIP Flood Damage Cost Calculator (accessed on 3 September 2024) provided damage costs by inundation depth for 0.025 to 1.219 *m*. It was assumed that an inundation depth of 2.743 *m* creates a complete loss and that the value of each house is \$750,000. Cost estimates for inundation depths between 1.219 and 2.743 *m* were linearly interpolated. Table S2 provides a listing of point values used to interpolate the curve.

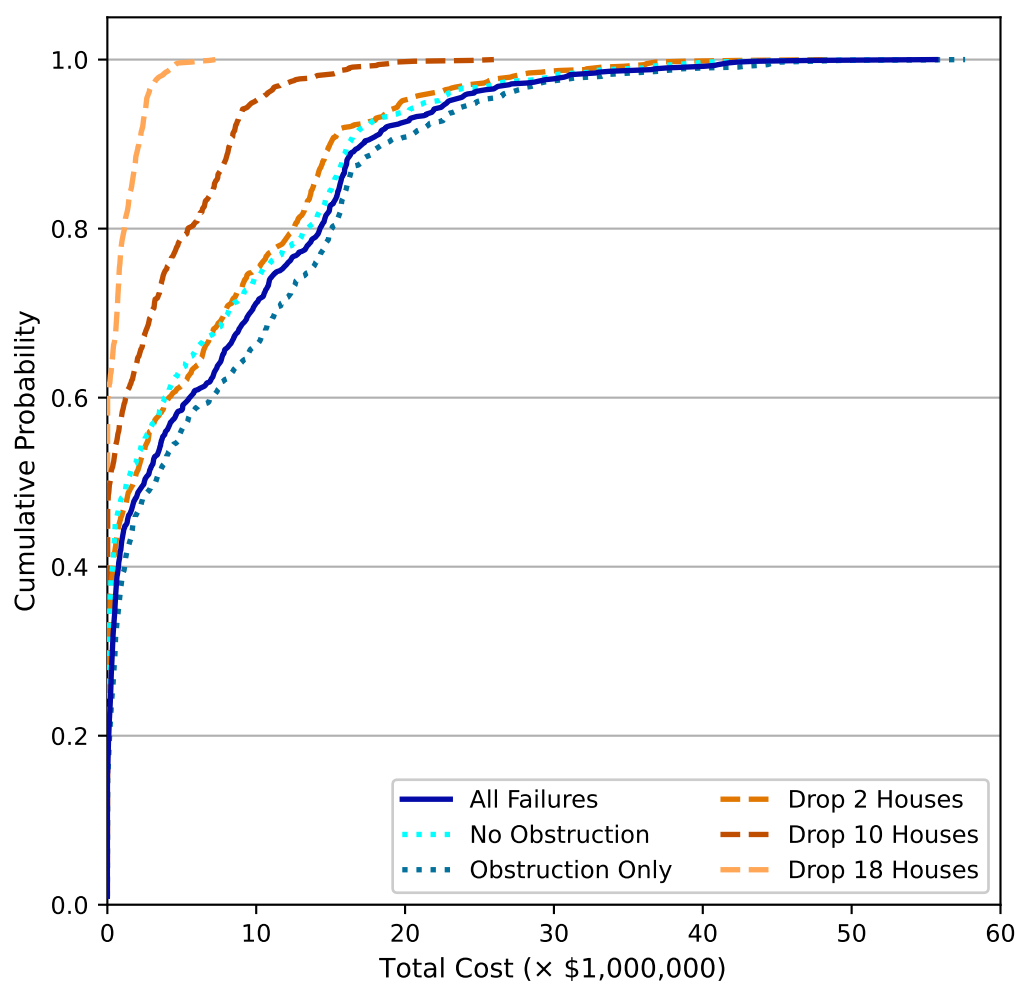


Figure 10. Cumulative probability for total climate realization damage cost. “All Failures” are the averaged total costs from “Stochastic Obstruction Depth” and “No Obstruction” branches of the Figure 4 event tree. Total averaged cost is determined because each initiating event is evaluated twice, one time for each “obstruction” branch, and it provides normalization for comparison with results from each branch. “No Obstruction” provides the likelihood of total cost from the “No Obstruction” branch, and “Obstruction Only” displays cumulative probability of total cost from the “Stochastic Obstruction Depth” branch. “Drop 2 Houses” is the cumulative probability of damage cost when houses #22 and #33, which are closest to the bridge, are removed from the “All Failures” damage cost calculations. “Drop 4 Houses” is the likelihoods for total damage cost when houses #21, #22, #32, and #33 are removed.

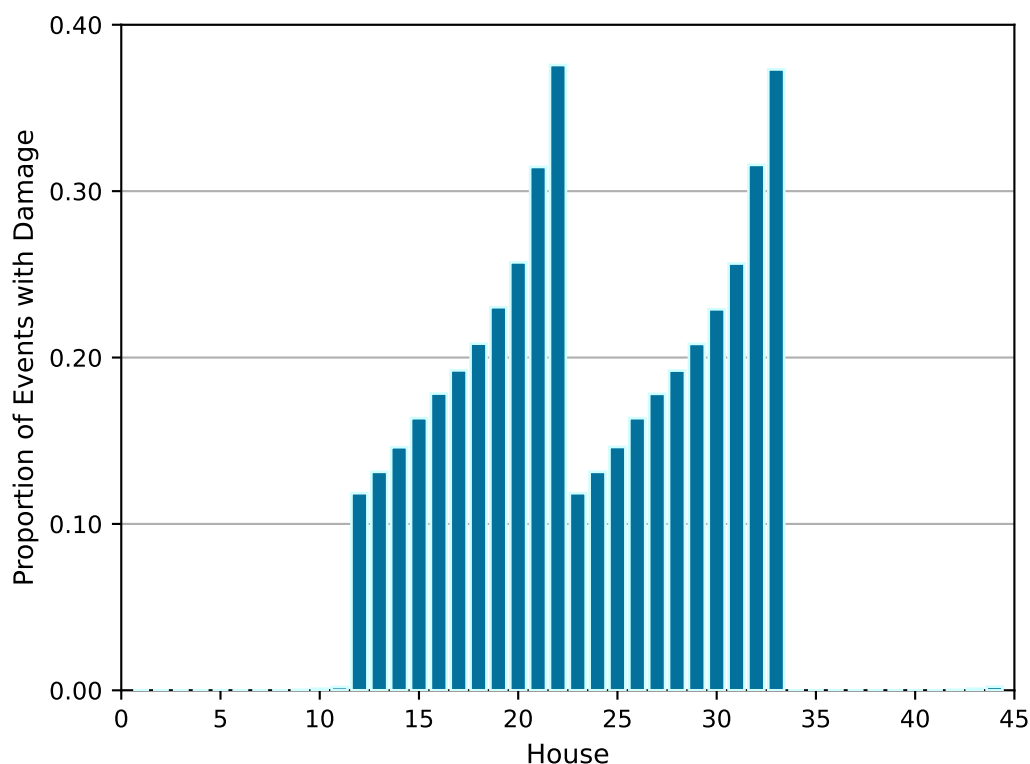


Figure 11. Likelihood for flooding by house. The houses that are closest to both the bridge and the channel center line are most likely to flood given the site layout, see Figure 5. The two closest houses are House #22 and #33, which are damaged in over 35% of the events evaluated. For the “Drop 2 Houses” scenario examined on Figure 10, Houses #22 and #33 are the two houses dropped from the analysis because these are the two houses most likely to flood. Damage likelihood decreases moving upstream within the lines of houses closest to the channel. For example, Houses #21 and #32 are damaged in over 30% of evaluated events. House #21 is immediately upstream of House #22 on the left bank, and House #32 is immediately upstream of House #33 on the right bank. In the “Drop 4 Houses” scenario listed on Table 2, Houses #21, #22, #32, and #33 are removed from total cost calculations because these are the four most likely houses to be damaged. For the second line of houses, which is the farthest from the channel center line, Houses #11 and #44 are most likely to flood because they are closest to the bridge. In the maximum water surface elevation simulation, which is shown on Figure S3 Panel (b), only second line Houses #9, #10, #11, #42, #43, and #44 are damaged.